

A coupled HDG/DG method for porous media with conducting/sealing faults

A. Cesmelioglu* M. Kuchta† J. J. Lee‡ S. Rhebergen§

February 18, 2025

Abstract

We introduce and analyze a coupled hybridizable discontinuous Galerkin/discontinuous Galerkin (HDG/DG) method for porous media in which we allow fully and partly immersed faults, and faults that separate the domain into two disjoint subdomains. We prove well-posedness and present an a priori error analysis of the discretization. Numerical examples verify our analysis.

1 Introduction

Subsurface flow problems are of interest to many areas of science and engineering such as geophysics, environmental sciences, hydrocarbon extraction, and geothermal energy production. Faults are geological structures that are discontinuities of displacement. In subsurface flow problems, faults can act as conduits or barriers to fluid flow, depending on the permeability on faults. These fault structures can cause significant changes in fluid flows, so understanding the interplay of faults (as conduits or as barriers) and fluid flows is important for applications. For the remainder of this paper we will refer to conduits (often called fractures) as *conducting faults* and barriers as *sealing faults*.

A mathematical model of subsurface flows with conducting and sealing faults was proposed in [27]. They furthermore analyzed a mixed finite element method for this problem. After this seminal work, numerous works on discretizing subsurface flows with faults have appeared in the literature. These include the hybrid high order method [11], the interior penalty discontinuous Galerkin method [25], staggered discontinuous Galerkin methods [31], a hybridized interior penalty method [23], a mixed virtual element method [5], a discrete finite volume method [24], a cut finite element method [9], a multipoint flux approximation method [10], a mixed hybrid mortar method [28, 29], and a finite volume method [12].

The Darcy equations for the porous-matrix flow are defined on a dim -dimensional domain. Fluid flow in faults, however, are modelled as flow problems on $(\text{dim} - 1)$ -dimensional domains. In this paper, to discretize this inter-dimensional problem, we propose a coupled dual mixed hybridizable discontinuous Galerkin (HDG) method and interior penalty discontinuous Galerkin (IPDG) method. The HDG method was originally introduced in [14] as an approach to reduce the computational costs of traditional discontinuous Galerkin methods. This was achieved by introducing new face unknowns in the discretization in such a way as to facilitate static condensation. The introduction of these new face unknowns, defined on $(\text{dim} - 1)$ -dimensional faces of the mesh, and their coupling to cell unknowns defined on dim -dimensional cells of the mesh, however, also presents a natural framework to deal with the inter-dimensional problem of porous-matrix flow with flow in faults. The dim -dimensional Darcy equations for the porous-matrix flow are discretized using the dual

*Department of Mathematics and Statistics, Oakland University, MI, USA (cesmelio@oakland.edu), <https://orcid.org/0000-0001-8057-6349>

†Simula Research Laboratory, Oslo, Norway (miroslav@simula.no), <https://orcid.org/0000-0002-3832-0988>

‡Department of Mathematics, Baylor University, TX, USA (jeonghun_lee@baylor.edu), <https://orcid.org/0000-0001-5201-8526>

§Department of Applied Mathematics, University of Waterloo, ON, Canada (srheberg@uwaterloo.ca), <http://orcid.org/0000-0001-6036-0356>

mixed HDG method (also called the LDG-H method in [14]). On $(\dim - 1)$ -dimensional conducting faults we discretize the flow equations using the IPDG method [3, 2]. The coupling between the \dim -dimensional HDG and $(\dim - 1)$ -dimensional IPDG method is handled automatically by the HDG framework. Finally, sealing faults are easily included in the HDG discretization as modified interface conditions.

This paper is organized as follows. In sections 2 and 3 we introduce the governing equations and its coupled HDG/DG finite element discretization, respectively. In sections 4 and 5, we prove well-posedness of the discretization and present an a priori error estimate for the numerical solution. Finally, in section 6 we present numerical results which include test cases that illustrate our theoretical analysis, as well as some benchmark test cases. We conclude in section 7.

2 Porous media with faults

Let Ω be an open, bounded, connected domain in \mathbb{R}^{\dim} with $\dim \in \{2, 3\}$. Let Γ_c, Γ_s be unions of disjoint $(\dim - 1)$ -dimensional piecewise linear submanifolds in Ω . We will refer to Γ_c as a conducting fault and Γ_s as a sealing fault. Denote by $\partial\Omega$ the polygonal/polyhedral boundary of Ω and by $\partial\Gamma_j$ the boundary of Γ_j , $j = c, s$. We will consider faults that are fully immersed in Ω (if $x \in \partial\Gamma_j$ then $x \notin \partial\Omega$), partly immersed in Ω (there exist $x, y \in \partial\Gamma_j$ such that $x \in \partial\Omega$ and $y \notin \partial\Omega$), and faults that separate the domain into two disjoint subdomains (if $x \in \partial\Gamma_j$ then $x \in \partial\Omega$). Let $\hat{\Omega} := \Omega \setminus (\Gamma_c \cup \Gamma_s)$ and n denote the outward unit normal vector to Ω .

Let γ be a subset of Γ_j , $j = c, s$, of positive $(\dim - 1)$ -dimensional Lebesgue measure which is obtained by the intersection of a $(\dim - 1)$ -dimensional plane and Γ_j , and let $\Omega_+^\gamma, \Omega_-^\gamma$ be two disjoint subdomains in Ω such that $\gamma = \partial\Omega_+^\gamma \cap \partial\Omega_-^\gamma$. On γ , n_\pm is the unit outward normal vector field on $\partial\Omega_\pm^\gamma$. Note that n_+ (n_- , resp.) is independent of the choice of Ω_+^γ (Ω_-^γ , resp.). Let $v \in [L^2(\Omega_+^\gamma \cup \Omega_-^\gamma)]^{\dim}$ be such that its traces on γ from Ω_\pm^γ , denoted by v_\pm , lie in $[L^2(\gamma)]^{\dim}$. Then, we define $\llbracket v \cdot n \rrbracket_\gamma := (v_+ - v_-) \cdot n_+$, $\{\!\{ v \cdot n \}\!\}_\gamma := \frac{1}{2}(v_+ + v_-) \cdot n_+$. Similarly, let $q \in L^2(\Omega_+^\gamma \cup \Omega_-^\gamma)$ such that its traces on γ from Ω_\pm^γ , denoted by q_\pm , lie in $L^2(\gamma)$. Then $\llbracket q \rrbracket_\gamma := q_+ - q_-$, $\{\!\{ q \}\!\}_\gamma := \frac{1}{2}(q_+ + q_-)$. Note that $\llbracket v \cdot n \rrbracket_\gamma$, $\{\!\{ v \cdot n \}\!\}_\gamma$, $\llbracket q \rrbracket_\gamma$, $\{\!\{ q \}\!\}_\gamma$ are independent of the choices of $\Omega_+^\gamma, \Omega_-^\gamma$. If γ is clear from the context, then we will write $\llbracket v \cdot n \rrbracket$, $\{\!\{ v \cdot n \}\!\}$, $\llbracket q \rrbracket$, $\{\!\{ q \}\!\}$ for simplicity. We depict the domain notation in fig. 1.

In Ω we denote the Darcy velocity by u , the pressure by p , a source term by g , and the permeability tensor by κ . Following [27], we will assume that κ is diagonal and there exist constants $\kappa_{\min}, \kappa_{\max}$ such that $0 < \kappa_{\min} \leq \kappa_{jj} \leq \kappa_{\max}$ for $j = 1, \dots, \dim$ almost everywhere in Ω .

The velocity, pressure, permeability, and source/sink term in the fault Γ_c are denoted by $u_f, p_f, \bar{\kappa}_f$, and g_f , respectively. Next, suppose that a unit normal vector n at $x \in \Gamma_c \cup \Gamma_s$ is uniquely determined up to orientation and define $\bar{\kappa}_{f,n}(x) := \kappa(x)n \cdot n$. Let τ_i , $1 \leq i \leq \dim$ be an orthonormal basis of the tangent space along $\Gamma_c \cup \Gamma_s$ at x . We can write $\bar{\kappa}_{f,\tau}(x)$ in terms of this basis: $\bar{\kappa}_{f,\tau}(x) = \sum_{i=1}^{\dim-1} \bar{\kappa}_i(x)\tau_i \otimes \tau_i$ with $\bar{\kappa}_i(x)$ the expansion coefficients. Then, for almost all $x \in \Gamma_c \cup \Gamma_s$, we assume that $\kappa(x) = \bar{\kappa}_{f,n}(x)n \otimes n + \bar{\kappa}_{f,\tau}(x)$. We further assume that $\kappa_{\min} \leq \bar{\kappa}_{f,n}(x), \bar{\kappa}_i(x) \leq \kappa_{\max}$ for almost all x . Finally, we define $\kappa_f := \bar{\kappa}_{f,\tau}d$ and $\alpha_f := 2\bar{\kappa}_{f,n}/d$, where d is the thickness of the fault.

The porous media model with conducting fault Γ_c (cf. [27]) and sealing fault Γ_s (cf. [22]), is now given by:

$$\kappa^{-1}u + \nabla p = 0 \quad \text{in } \hat{\Omega}, \quad (1a)$$

$$\nabla \cdot u = g \quad \text{in } \hat{\Omega}, \quad (1b)$$

$$-\nabla_\tau \cdot (\kappa_f \nabla_\tau p_f) = g_f + \llbracket u \cdot n \rrbracket \quad \text{in } \Gamma_c, \quad (1c)$$

$$-\xi u_+ \cdot n_+ + \alpha_f p_+ = \alpha_f p_f - (1 - \xi)u_- \cdot n_- \quad \text{in } \Gamma_c, \quad (1d)$$

$$-\xi u_- \cdot n_- + \alpha_f p_- = \alpha_f p_f - (1 - \xi)u_+ \cdot n_+ \quad \text{in } \Gamma_c, \quad (1e)$$

$$2\{\!\{ u \cdot n \}\!\} = \alpha_f \llbracket p \rrbracket \quad \text{in } \Gamma_s, \quad (1f)$$

$$\llbracket u \cdot n \rrbracket = 0 \quad \text{in } \Gamma_s, \quad (1g)$$

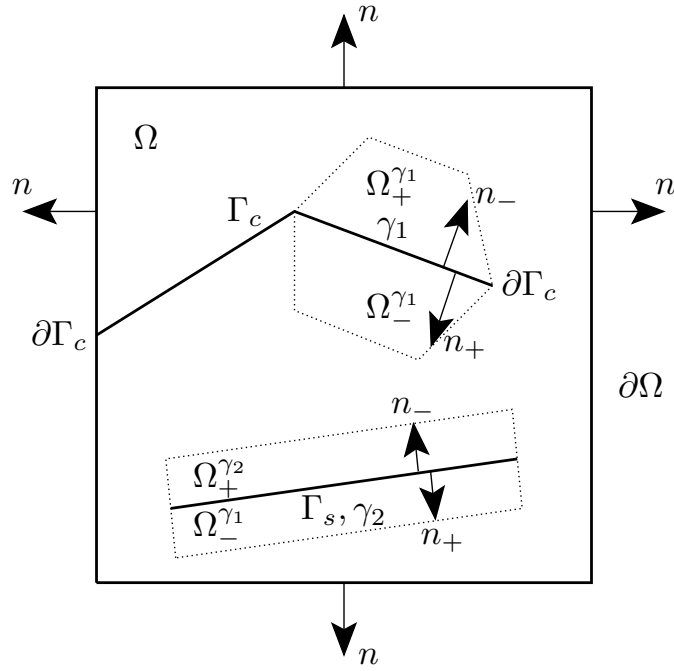


Figure 1: Illustration of the domain notation in \mathbb{R}^2 .

where $1/2 < \xi \leq 1$ is a constant and where ∇_τ and $\nabla_\tau \cdot$ are the tangential gradient and divergence operators along Γ_c .

The boundary of the conducting fault Γ_c is partitioned into a Neumann part and a Dirichlet part. These are denoted by $(\partial\Gamma_c)^N$ and $(\partial\Gamma_c)^D$, respectively. Let p^D be a given pressure on $\partial\Omega$, let p_f^D be a given pressure on $(\partial\Gamma_c)^D$, and let g_f^N be given Neumann boundary data on $(\partial\Gamma_c)^N$. We then consider the following boundary conditions:

$$p = p^D \quad \text{on } \partial\Omega, \quad (2a)$$

$$-\kappa_f \nabla_\tau p_f = g_f^N \quad \text{on } (\partial\Gamma_c)^N, \quad (2b)$$

$$p_f = p_f^D \quad \text{on } (\partial\Gamma_c)^D. \quad (2c)$$

3 The discretization

Let \mathcal{T} be a shape-regular (cf. [7]) triangulation of the domain Ω into non-overlapping simplices K that aligns with the faults. The set of all $(\dim - 1)$ -dimensional faces of ∂K , for $K \in \mathcal{T}$, is denoted by \mathcal{F} . We assume that the intersection of Γ_j and \mathcal{F} gives a triangulation of Γ_j for $j = c, s$. For a k -dimensional simplex S , h_S is the diameter of the smallest k -dimensional ball containing S , and we define $h := \max_{K \in \mathcal{T}} h_K$. The outward unit normal vector field on ∂K for a simplex K is denoted by n_K . However, if K is clear from the context, we will simply write n .

We split \mathcal{F} into four sets; \mathcal{F}_b for the boundary faces, \mathcal{F}_c^f and \mathcal{F}_s^f for the faces on the conducting and sealing faults, respectively, and \mathcal{F}_0 for the interior faces that are not on the faults. In other words,

$$\begin{aligned} \mathcal{F}_j^f &:= \{F \in \mathcal{F} : F \subset \Gamma_j\}, \quad j = s, c, & \mathcal{F}_b &:= \{F \in \mathcal{F} : F \subset \partial\Omega\}, \\ \mathcal{F}_0 &:= \mathcal{F} \setminus (\mathcal{F}_c^f \cup \mathcal{F}_s^f \cup \mathcal{F}_b). \end{aligned}$$

We will also denote the union of all faces in \mathcal{F}_0 by $\Gamma_0 := \bigcup_{F \in \mathcal{F}_0} F$. Let $F^+, F^- \in \mathcal{F}_c^f$ be two adjacent faces on the conducting fault Γ_c . These faces share e , an interior edge when $\dim = 3$ and a vertex when $\dim = 2$. An

edge/vertex of a face $F \in \mathcal{F}_c^f$ that lies on $\partial\Gamma_c$ is considered as a boundary edge/vertex. The set of all interior edges/vertices on the conducting fault Γ_c is denoted by $\mathcal{E}_c^{f,int}$ while the sets of edges/vertices on $(\partial\Gamma_c)^N$ and $(\partial\Gamma_c)^D$ are denoted by $\mathcal{E}_c^{f,N}$ and $\mathcal{E}_c^{f,D}$, respectively. Furthermore, we define $\mathcal{E}_c^{f,int,D} := \mathcal{E}_c^{f,int} \cup \mathcal{E}_c^{f,D}$.

The outward unit normal vector to a face $F \in \mathcal{F}_c^f$ on one of its vertices ($\dim = 2$) or edges ($\dim = 3$) e is denoted by n_e , which reduces to ± 1 if $\dim = 2$. For $e \in \mathcal{E}_c^{f,int}$ shared by faces $F_+, F_- \in \mathcal{F}_c^f$, we define

$$\tilde{h}_e := \begin{cases} h_e & \text{if } \dim = 3, \\ \max(h_{F_+}, h_{F_-}) & \text{if } \dim = 2. \end{cases} \quad (3)$$

We define the jump and average operators across an interior edge e shared by faces $F_+, F_- \in \mathcal{F}_c^f$ as $[[pn]]_e := p_+n_{e,+} + p_-n_{e,-}$ and $\{\{p\}\}_e := (p_+ + p_-)/2$, respectively. Here p_\pm is the trace of $p|_{F_\pm}$ restricted to e . On a boundary edge $e \in \partial\Gamma_c$ we define $[[pn]]_e := pn_e$ and $\{\{p\}\}_e := p$ with n_e the outward unit normal vector on e to Γ_c .

For the discretization of the porous medium with faults problem eqs. (1) and (2) we consider the following finite element spaces:

$$\begin{aligned} V_h &:= \{v_h \in [L^2(\Omega)]^{\dim} : v_h \in [P_k(K)]^{\dim} \forall K \in \mathcal{T}\}, \\ Q_h &:= \{q_h \in L^2(\Omega) : q_h \in P_k(K) \forall K \in \mathcal{T}\}, \\ Q_h^f &:= \{q_h^f \in L^2(\Gamma_c) : q_h^f \in P_{k_f}(F) \forall F \in \mathcal{F}_c^f\}, \quad k_f = k, k+1, \\ \bar{Q}_h &:= \{\bar{q}_h \in L^2((\cup_{F \in \mathcal{F}_c^f} F) \setminus \Gamma_c) : \bar{q}_h \in P_k(F) \forall F \in \mathcal{F} \setminus \mathcal{F}_c^f\}, \\ \bar{Q}_h(w) &:= \{\bar{q}_h \in \bar{Q}_h : \bar{q}_h = \bar{\Pi}_h w \text{ on } \partial\Omega\}, \forall w \in L^2(\partial\Omega), \\ \mathbf{Q}_h(w) &:= Q_h \times \bar{Q}_h(w) \times Q_h^f, \end{aligned} \quad (4)$$

where $P_l(R)$ denotes the space of polynomials of degree $l \geq 1$ on a domain R and $\bar{\Pi}_h$ is the L^2 -projection into $\{\bar{q}_h \in L^2(\partial\Omega) : \bar{q}_h \in P_k(F) \forall F \in \mathcal{F}_\partial\}$ where \mathcal{F}_∂ is the set of all faces that lie on $\partial\Omega$. Elements in $\mathbf{Q}_h(w)$ will be denoted by $\mathbf{q}_h = (q, \bar{q}, q^f)$.

To write the coupled HDG/DG discretization we introduce bilinear forms

$$\begin{aligned} a_h(\cdot, \cdot) &: V_h \times V_h \rightarrow \mathbb{R}, & b_h(\cdot, \cdot) &: V_h \times \mathbf{Q}_h(w) \rightarrow \mathbb{R}, \\ c_h^f(\cdot, \cdot) &: Q_h^f \times Q_h^f \rightarrow \mathbb{R}, & c_h(\cdot, \cdot) &: \mathbf{Q}_h(w) \times \mathbf{Q}_h(w) \rightarrow \mathbb{R} \end{aligned}$$

by

$$a_h(w, v) := \sum_{K \in \mathcal{T}} \int_K \kappa^{-1} w \cdot v \, dx + \sum_{F \in \mathcal{F}_c^f} \int_F 2\alpha_f^{-1} \{\{w \cdot n\}\} \{\{v \cdot n\}\} \, ds \quad (5a)$$

$$+ \sum_{F \in \mathcal{F}_c^f} \int_F \alpha_f^{-1} \left((\xi - \frac{1}{2}) [[w \cdot n]] [[v \cdot n]] + 2 \{\{w \cdot n\}\} \{\{v \cdot n\}\} \right) \, ds,$$

$$b_h(v, \mathbf{q}) := - \sum_{K \in \mathcal{T}} \int_K q \nabla \cdot v \, dx + \sum_{K \in \mathcal{T}} \int_{\partial K \setminus \Gamma_c} \bar{q} v \cdot n \, ds + \sum_{F \in \mathcal{F}_c^f} \int_F q_f [v \cdot n] \, ds, \quad (5b)$$

$$c_h^f(r, q) := \sum_{F \in \mathcal{F}_c^f} \int_F \kappa_f \nabla_\tau r \cdot \nabla_\tau q \, ds + \sum_{e \in \mathcal{E}_c^{f,int,D}} \int_e \frac{\sigma}{\tilde{h}_e} \{\{\kappa_f\}\}_e [r]_e [q]_e \, dl \quad (5c)$$

$$- \sum_{e \in \mathcal{E}_c^{f,int,D}} \int_e \{\{\kappa_f \nabla_\tau r\}\}_e \cdot [qn_e]_e \, dl - \sum_{e \in \mathcal{E}_c^{f,int,D}} \int_e \{\{\kappa_f \nabla_\tau q\}\}_e \cdot [rn_e]_e \, dl,$$

$$c_h(\mathbf{r}, \mathbf{q}) := c_h^f(r_f, q_f) + \sum_{K \in \mathcal{T}} \int_{\partial K \setminus (\Gamma_c \cup \Gamma_s)} \alpha (q - \bar{q})(r - \bar{r}) \, ds, \quad (5d)$$

where for any $K \in \mathcal{T}$, $\alpha \geq 0$ is piecewise constant on each $F \subset \partial K$ such that $\alpha \neq 0$ on at least one $F \subset \partial K$ and a linear functional $f_h : Q_h \times Q_h^f \rightarrow \mathbb{R}$ is defined as

$$\begin{aligned} f_h((q, q_f)) &:= \sum_{K \in \mathcal{T}} \int_K gq \, dx + \sum_{F \in \mathcal{F}_c^f} \int_F g_f q_f \, ds \\ &\quad - \sum_{e \in \mathcal{E}_c^{f,N}} \int_e q_f g_f^N \cdot n_e \, dl + \sum_{e \in \mathcal{E}_c^{f,D}} \int_e \left(\frac{\sigma}{\bar{h}_e} \kappa_f p_f^D q_f - \kappa_f \nabla_\tau q_f \cdot n_e p_f^D \right) dl. \end{aligned} \quad (6)$$

The coupled HDG/DG discretization for the fault problem eqs. (1) and (2) is now given by: Find $(\mathbf{u}_h, \mathbf{p}_h) \in \mathbf{V}_h \times \mathbf{Q}_h(p^D)$ such that

$$a_h(u_h, v_h) + b_h(v_h, \mathbf{p}_h) = 0 \quad \forall v_h \in V_h, \quad (7a)$$

$$-b_h(u_h, \mathbf{q}_h) + c_h(\mathbf{p}_h, \mathbf{q}_h) = f_h((q_h, q_{h,f})) \quad \forall \mathbf{q}_h \in \mathbf{Q}_h(0). \quad (7b)$$

The following lemma shows that the discretization eq. (7) is consistent.

Lemma 1 (Consistency). *Let $u \in [H^1(\hat{\Omega})]^{\dim}$, $p \in H^1(\hat{\Omega})$, and $p_f \in H^s(\Gamma_c)$ with $s > 3/2$ satisfy eqs. (1) and (2). Denote the average of p on $\mathcal{F}_0 \cup \mathcal{F}_s^f$ by $\{\{p\}\}$. Then u and $\mathbf{p} := (p, \{\{p\}\}, p_f)$ satisfy eq. (7).*

Proof. We will show that $R = 0$, where

$$R = a_h(u, v_h) + b_h(v_h, \mathbf{p}) - b_h(u, \mathbf{q}_h) + c_h(\mathbf{p}, \mathbf{q}_h) - f_h((q_h, q_{h,f})).$$

We first show that $a_h(u, v_h) + b_h(v_h, \mathbf{p}) = 0$. Multiply eq. (1a) by a test function $v_h \in V_h$, integrate over a cell $K \in \mathcal{T}$, integrate by parts, and sum over all simplices in \mathcal{T} :

$$\begin{aligned} \sum_{K \in \mathcal{T}} \int_K \kappa^{-1} u \cdot v_h \, dx - \sum_{K \in \mathcal{T}} \int_K p \nabla \cdot v_h \, dx + \sum_{K \in \mathcal{T}} \int_{\partial K \setminus (\Gamma_c \cup \Gamma_s)} p v_h \cdot n \, ds \\ + \sum_{K \in \mathcal{T}} \int_{\partial K \cap (\Gamma_s \cup \Gamma_c)} p v_h \cdot n \, ds = 0. \end{aligned}$$

On Γ_s and Γ_c , using the identity $p_+ v_{h,+} \cdot n_+ + p_- v_{h,-} \cdot n_- = \{\{p\}\} [v_h \cdot n] + [p] \{\{v_h \cdot n\}\}$, we have

$$\begin{aligned} \sum_{K \in \mathcal{T}} \int_K \kappa^{-1} u \cdot v_h \, dx - \sum_{K \in \mathcal{T}} \int_K p \nabla \cdot v_h \, dx + \sum_{K \in \mathcal{T}} \int_{\partial K \setminus (\Gamma_c \cup \Gamma_s)} p v_h \cdot n \, ds \\ + \int_{\Gamma_c \cup \Gamma_s} (\{\{p\}\} [v_h \cdot n] + [p] \{\{v_h \cdot n\}\}) \, ds = 0. \end{aligned} \quad (8)$$

By eq. (1f),

$$\int_{\Gamma_s} (\{\{p\}\} [v_h \cdot n] + [p] \{\{v_h \cdot n\}\}) \, ds = \int_{\Gamma_s} (\{\{p\}\} [v_h \cdot n] + 2\alpha_f^{-1} \{\{u \cdot n\}\} \{\{v_h \cdot n\}\}) \, ds. \quad (9)$$

Note that the sum and difference of eq. (1d) and eq. (1e) give, respectively,

$$(1 - 2\xi) [u \cdot n] + 2\alpha_f \{\{p\}\} = 2\alpha_f p_f, \quad \alpha_f [p] = 2\{\{u \cdot n\}\} \quad \text{on } \Gamma_c.$$

From these identities,

$$\begin{aligned} \int_{\Gamma_c} (\{\{p\}\} [v_h \cdot n] + [p] \{\{v_h \cdot n\}\}) \, ds &= \sum_{F \in \mathcal{F}_c^f} \int_F \alpha_f^{-1} \left((\xi - \frac{1}{2}) [u \cdot n] [v_h \cdot n] + 2\{\{u \cdot n\}\} \{\{v_h \cdot n\}\} \right) \, ds \\ &\quad + \int_{\Gamma_c} p_f [v_h \cdot n] \, ds. \end{aligned} \quad (10)$$

Combining eqs. (8) to (10), we obtain $a_h(u, v_h) + b_h(v_h, \mathbf{p}) = 0$.

To show $R = 0$ note that

$$-b_h(u, \mathbf{q}_h) + c_h(\mathbf{p}, \mathbf{q}_h) = - \sum_{F \in \mathcal{F}_c^f} \int_F \llbracket u \cdot n \rrbracket q_{h,f} \, ds + \sum_{K \in \mathcal{T}} \int_K g q \, dx + c_h^f(p_f, q_{h,f}) \quad (11)$$

because $u \cdot n$ is single-valued on $\mathcal{F}_0 \cup \mathcal{F}_s^f$ by eq. (1g), and $\nabla \cdot u = g$ by eq. (1b). We also multiply eq. (1c) by a test function $q_{h,f} \in Q_h^f$, integrate over faces $F \in \mathcal{F}_c^f$, and sum over the faces to obtain

$$- \sum_{F \in \mathcal{F}_c^f} \int_F \nabla_\tau \cdot (\kappa_f \nabla_\tau p_f) q_{h,f} \, ds = \sum_{F \in \mathcal{F}_c^f} \int_F g_f q_{h,f} \, ds + \sum_{F \in \mathcal{F}_c^f} \int_F \llbracket u \cdot n \rrbracket q_{h,f} \, ds.$$

Recall the definition of \tilde{h}_e in (3). Integrating by parts and using the symmetric interior penalty DG method (see, for example, [30]) we obtain:

$$\begin{aligned} c_h^f(p_f, q_{h,f}) &= \sum_{F \in \mathcal{F}_c^f} \int_F \kappa_f \nabla_\tau p_f \cdot \nabla_\tau q_{h,f} \, ds + \sum_{e \in \mathcal{E}_c^{f,int,D}} \int_e \frac{\sigma}{\tilde{h}_e} \{\kappa_f\} \llbracket p_f \rrbracket \llbracket q_{h,f} \rrbracket \, dl \\ &\quad - \sum_{e \in \mathcal{E}_c^{f,int,D}} \int_e \{\kappa_f \nabla_\tau p_f\} \cdot \llbracket q_{h,f} n_e \rrbracket \, dl - \sum_{e \in \mathcal{E}_c^{f,int,D}} \int_e \{\kappa_f \nabla_\tau q_{h,f}\} \cdot \llbracket p_f n_e \rrbracket \, dl \\ &= \sum_{F \in \mathcal{F}_c^f} \int_F g_f q_{h,f} \, ds + \sum_{F \in \mathcal{F}_c^f} \int_F \llbracket u \cdot n \rrbracket q_{h,f} \, ds - \sum_{e \in \mathcal{E}_c^{f,N}} \int_e q_{h,f} g_f^N \cdot n_e \, dl \\ &\quad + \sum_{e \in \mathcal{E}_c^{f,D}} \int_e \left(\frac{\sigma}{\tilde{h}_e} \kappa_f p_f^D q_{h,f} - \kappa_f \nabla_\tau q_{h,f} \cdot n_e p_f^D \right) \, dl. \end{aligned} \quad (12)$$

Combining eq. (11) and eq. (12), we conclude that $R = 0$. \square

4 Well-posedness of the discrete problem

In this section we assume that $p^D = 0$ on $\partial\Omega$ for simplicity of presentation. For general boundary condition $p^D \neq 0$ we can recast eq. (7) to an equivalent problem finding $(u_h, \mathbf{p}_h^0) \in V_h \times \mathbf{Q}_h(0)$ with the same bilinear forms but with modified right-hand sides. To simplify notation in this section, we will write \mathbf{Q}_h instead of $\mathbf{Q}_h(0)$.

For the analysis in this and the following sections we define the following norms:

$$\begin{aligned} \|v\|_{V_h}^2 &:= \|v\|_\Omega^2 + \sum_{F \in \mathcal{F}_c^f} \left(\|\llbracket v \cdot n \rrbracket\|_F^2 + \|\{\{v \cdot n\}\}\|_F^2 \right) + \sum_{F \in \mathcal{F}_s^f} \|\{\{v \cdot n\}\}\|_F^2 \quad \forall v \in V_h, \\ \|q_f\|_{Q_{h,f}}^2 &:= \sum_{F \in \mathcal{F}_c^f} \|\nabla_\tau q_f\|_F^2 + \sum_{e \in \mathcal{E}_c^{f,int,D}} \frac{1}{\tilde{h}_e} \|\llbracket q_f \rrbracket\|_e^2 \quad \forall q_f \in Q_h^f + H^1(\Gamma_c). \end{aligned}$$

Lemma 2 (Coercivity and boundedness of a_h). *The bilinear form a_h is bounded and coercive on V_h , that is,*

$$a_h(v_h, v_h) \geq \min \{ \kappa_{\max}^{-1}, \alpha_f^{-1} (\xi - \frac{1}{2}) \} \|v_h\|_{V_h}^2 \quad \forall v_h \in V_h, \quad (13a)$$

$$a_h(u_h, v_h) \leq \max \{ \kappa_{\min}^{-1}, 2\alpha_f^{-1} \} \|u_h\|_{V_h} \|v_h\|_{V_h} \quad \forall u_h, v_h \in V_h. \quad (13b)$$

Proof. Equation (13a) is straightforward by the definitions of a_h and $\|\cdot\|_{V_h}$. The proof of eq. (13b) in addition uses the Cauchy–Schwarz inequality and the assumption that $\xi \leq 1$. \square

Lemma 3 (c_h is positive semi-definite). *For sufficiently large penalty parameter $\sigma > 0$,*

$$c_h(\mathbf{q}_h, \mathbf{q}_h) \geq C\kappa_{\min} \|q_{h,f}\|_{Q_{h,f}}^2 + \alpha \sum_{K \in \mathcal{T}} \|q_h - \bar{q}_h\|_{\partial K \setminus (\Gamma_c \cup \Gamma_s)}^2 \quad \forall \mathbf{q}_h \in \mathbf{Q}_h,$$

where C depends on a discrete trace inequality constant and the penalty parameter σ .

Proof. First note that for sufficiently large $\sigma > 0$ we have (see, for example, [16, Lemma 4.12]),

$$c_h^f(q_{h,f}, q_{h,f}) \geq C\kappa_{\min} \|q_{h,f}\|_{Q_{h,f}}^2.$$

The result follows noting that

$$c_h(\mathbf{q}_h, \mathbf{q}_h) = c_h^f(q_{h,f}, q_{h,f}) + \sum_{K \in \mathcal{T}} \int_{\partial K \setminus (\Gamma_c \cup \Gamma_s)} \alpha (q_h - \bar{q}_h)^2 ds.$$

□

The following result, proven in [13, Proposition 2.1], will be used to prove Theorem 1, i.e., the well-posedness of eq. (7).

Lemma 4. *Suppose that $w \in [H^1(K)]^{\dim}$ for a simplex $K \in \mathcal{T}$. For a fixed face F of K , there exists a unique linear interpolation $\tilde{\Pi}_K^F : [H^1(K)]^{\dim} \rightarrow [P_k(K)]^{\dim}$ such that*

$$\int_K (\tilde{\Pi}_K^F w - w) \cdot v dx = 0, \quad \forall v \in [P_{k-1}(K)]^{\dim}, \quad k \geq 1, \quad (14a)$$

$$\int_{F'} (\tilde{\Pi}_K^F w - w) \cdot nr ds = 0, \quad \forall r \in P_k(F'), \quad \forall \text{face } F' \subset \partial K, \quad F' \neq F. \quad (14b)$$

Moreover, for the same F and $\tilde{\Pi}_K^F$, if $w \in [H^{s+1}(K)]^{\dim}$, $0 \leq s \leq k$, then

$$\|\tilde{\Pi}_K^F w \cdot n - P_F w \cdot n\|_F \leq Ch_K^{s+1/2} \|P_K \nabla \cdot w\|_{H^s(K)}, \quad (15a)$$

$$\|\tilde{\Pi}_K^F w - w\|_K \leq Ch_K^{s+1} \|w\|_{H^{s+1}(K)}, \quad (15b)$$

where P_F is the L^2 -projection into $P_k(F)$ and P_K is the L^2 -projection into $P_k(K)$.

Theorem 1 (Well-posedness). *Suppose that each simplex $K \in \mathcal{T}$ has a face in \mathcal{F}_0 and each connected component of $\Omega \setminus \Gamma_c$ has a part of its boundary intersecting with $\partial\Omega$ with positive $(\dim - 1)$ -dimensional Lebesgue measure. For sufficiently large penalty parameter σ , the discrete problem eq. (7) is well-posed.*

Proof. To show well-posedness of the finite-dimensional linear problem eq. (7), it is sufficient to show uniqueness. For this, let $g_f = 0$ in Γ_c , $g = 0$ in $\hat{\Omega}$, $p_f^D = 0$ on $(\partial\Gamma_c)^D$, and $g_f^N = 0$ on $(\partial\Gamma_c)^N$, choose $v_h = u_h$ and $\mathbf{q}_h = \mathbf{p}_h$ in eq. (7), and add eqs. (7a) and (7b) to find $a_h(u_h, u_h) + c_h(\mathbf{p}_h, \mathbf{p}_h) = 0$. The coercivity $a_h(u_h, u_h) \geq \kappa_{\max}^{-1} \|u_h\|_{\hat{\Omega}}^2$ by eq. (13a) and positive semi-definiteness of c_h by lemma 3 immediately imply that $u_h = 0$ in Ω , that $p_{h,f} = 0$ in Γ_c , that $p_h = \bar{p}_h$ for all $F \in \mathcal{F}_0$ and since we assumed $p^D = 0$, that $p_h = \bar{p}_h = 0$ for all $F \in \mathcal{F}_b$. We are therefore left to show that $p_h = 0$ in Ω and $\bar{p}_h = 0$ on all $F \in \mathcal{F}_0 \cup \mathcal{F}_s^f$. To show this, first observe that since $u_h = 0$ and $p_{h,f} = 0$ after integrating by parts in eq. (7a), we obtain

$$\sum_{K \in \mathcal{T}} \int_K \nabla p_h \cdot v_h dx - \sum_{K \in \mathcal{T}} \int_{\partial K} p_h v_h \cdot n ds + \sum_{K \in \mathcal{T}} \int_{\partial K \setminus \Gamma_c} \bar{p}_h v_h \cdot n ds = 0 \quad \forall v_h \in V_h. \quad (16)$$

Next, we let $K \in \mathcal{T}$, and let $F \subset \partial K$ be a face such that $F \in \mathcal{F}_0$. By the existence of $\tilde{\Pi}_K^F$ in lemma 4, there exists $v_h^K \in [P_k(K)]^{\dim}$ such that $v_h^K \cdot n = 0$ on any face $F' \subset \partial K$, $F' \neq F$, and

$$\int_K v_h^K \cdot w_h dx = \int_K \nabla p_h \cdot w_h dx \quad \forall w_h \in [P_{k-1}(K)]^{\dim}.$$

Given $K \in \mathcal{T}$ choose $v_h \in V_h$ such that

$$v_h = \begin{cases} v_h^K & \text{on } K, \\ 0 & \text{otherwise.} \end{cases} \quad (17)$$

Choosing v_h in eq. (16) as described by eq. (17) and using that $p_h = \bar{p}_h$ for all $F \in \mathcal{F}_0 \cup \mathcal{F}_b$, we find

$$b_h(v_h, \mathbf{p}_h) = \int_K \nabla p_h \cdot \nabla p_h \, dx = 0. \quad (18)$$

Therefore, $\nabla p_h = 0$ on K which implies that p_h is a constant on K . Since $K \in \mathcal{T}$ is arbitrary, p_h is element-wise constant on Ω .

Finally, let $F_s \in \mathcal{F}_s^f$. Then, $F_s = \partial K_1 \cap \partial K_2$ for some $K_1, K_2 \in \mathcal{T}$. This time we define $v_h \in V_h$ such that it vanishes on $\Omega \setminus (K_1 \cup K_2)$ and such that its normal component takes the following facial values as a function on K_i :

$$v_h \cdot n|_F = \begin{cases} -p_h|_{K_i} + \bar{p}_h & \text{if } F = F_s \\ 0 & \text{if } F \neq F_s \end{cases} \quad \text{for } i = 1, 2, \quad (19)$$

and all other local BDM degrees of freedom vanish. Using this v_h in eq. (16) together with the fact that $\nabla p_h = 0$ element-wise on Ω , we obtain that $p_h = \bar{p}_h$ on F_s . Since $F_s \in \mathcal{F}_s^f$ is arbitrary, we conclude that $p_h = \bar{p}_h$ on Γ_s . Furthermore, since p_h is constant on every $K \in \mathcal{T}$, using that $p_h = \bar{p}_h$ on all faces in $\mathcal{F}_0 \cup \mathcal{F}_s^f$ we conclude that p_h and \bar{p}_h are constant on each connected component of $\Omega \setminus \Gamma_c$. Recalling that $\bar{p}_h = 0$ on \mathcal{F}_b , p_h and \bar{p}_h must also vanish and so eq. (7) has a unique solution. \square

Remark 1. We assume that every connected component of $\Omega \setminus \Gamma_c$ has a boundary part intersecting with $\partial\Omega$. If this is not true, then there are connected components whose boundaries are included in Γ_c . For simplicity of presentation, assume that there is only one such connected component Ω_0 . Then, the compatibility condition $\int_{\partial\Omega_0} u \cdot n \, ds = \int_{\Omega_0} \nabla \cdot u \, dx$ is necessary as in pure Neumann boundary condition problems. Its discretization needs a modified bilinear form with Lagrange multiplier $q_0 \in \mathbb{R}$ where $\tilde{b}_h(v_h, \tilde{\mathbf{q}}_h) = b_h(v_h, \mathbf{q}_h) + q_0(\int_{\Omega_0} \nabla \cdot v_h \, dx - \int_{\partial\Omega_0} v_h \cdot n \, ds)$ and $\tilde{\mathbf{q}}_h = (q_h, \bar{q}_h, q_{h,f}, q_{h,0}) \in \mathbf{Q}_h \times \mathbb{R}$. For well-posedness we can obtain $u_h = 0$, $p_{h,f} = 0$, and $\bar{p}_h = 0$ on \mathcal{F}_0 by the same argument. We can also obtain that p_h is element-wise constant by the same argument as in eq. (18) by using the v_h defined in eq. (17). On the connected component $\Omega \setminus \bar{\Omega}_0$, we can show $p_h = 0$, $\bar{p}_h = 0$ as in the proof of theorem 1, so it suffices to show $p_h = \bar{p}_h = p_{h,0} = 0$ on Ω_0 . For $F \in \mathcal{F}_0 \cap \Omega_0$, by taking the test function as in eq. (19) with the right-hand side quantity replaced by $p_h|_{K_i} + p_{h,0}$, we can show that $p_h = -p_{h,0}$ on Ω_0 because we assume that every $K \in \mathcal{T}$ contains a face in \mathcal{F}_0 . Then, $\tilde{b}_h(v_h, \tilde{\mathbf{p}}_h) = 0$ is reduced to $\sum_{K \in \mathcal{T}, K \subset \Omega_0} \int_{\partial K \cap \Gamma_s} \bar{p}_h v_h \cdot n \, ds + p_{h,0} \int_{\partial\Omega_0} v_h \cdot n \, ds = 0$. Taking v_h as an arbitrary constant vector on Ω_0 implies $p_{h,0} = p_h = 0$ and taking the test function as in eq. (19) implies $\bar{p}_h = 0$.

5 Error Analysis

In this section we prove a priori error estimates for the solution of our HDG/DG discretization defined by eq. (7).

We begin with defining an interpolation operator. On Q_h and V_h we consider the HDG projection $(\Pi v, \Pi q) \in [P_k(K)]^{\dim} \times P_k(K)$. This projection is defined on any $K \in \mathcal{T}$ and for any $(v, q) \in [H^1(K)]^{\dim} \times H^1(K)$ as follows (cf. [17, (3.4)]):

$$\int_K \Pi v \cdot \tilde{v} \, dx = \int_K v \cdot \tilde{v} \, dx \quad \forall \tilde{v} \in [P_{k-1}(K)]^{\dim}, \quad (20a)$$

$$\int_K \Pi q \tilde{q} \, dx = \int_K q \tilde{q} \, dx \quad \forall \tilde{q} \in P_{k-1}(K), \quad (20b)$$

$$\int_F (\Pi v \cdot n + \tilde{\alpha} \Pi q) r \, ds = \int_F (v \cdot n + \tilde{\alpha} q) r \, ds \quad \forall r \in P_k(F), F \subset \partial K, \quad (20c)$$

where $\tilde{\alpha} = \alpha$ if $F \subset \mathcal{F}_0 \cup \mathcal{F}_b$, and $\tilde{\alpha} = 0$ if $F \in \mathcal{F}_c^f \cup \mathcal{F}_s^f$. Note that Πv and Πq both depend on v and q , however, for notational simplicity we do not write down this dependence. Furthermore, let $\bar{\Pi}_Q$ be the L^2 -projection operator onto \bar{Q}_h , and let $\Pi_{Q^f} : H^s(\Gamma_c) \mapsto Q_h^f$, $s > 3/2$ be the following elliptic projection:

$$c_h^f(p^f, q_h^f) = c_h^f(\Pi_{Q^f} p^f, q_h^f) \quad \forall q_h^f \in Q_h^f. \quad (21)$$

We introduce the following decomposition of the errors:

$$\begin{aligned} e_u^I &= u - \Pi u, & e_u^h &= u_h - \Pi u, \\ e_p^I &= p - \Pi p, & e_p^h &= p_h - \Pi p, \\ \bar{e}_p^I &= \{\{p\}\} - \bar{\Pi}_Q \{\{p\}\}, & \bar{e}_p^h &= \bar{p}_h - \bar{\Pi}_Q \{\{p\}\}, \\ e_{p_f}^I &= p_f - \Pi_{Q^f} p_f, & e_{p_f}^h &= p_{h,f} - \Pi_{Q^f} p_f. \end{aligned} \quad (22)$$

We will use the following compact notation: $\mathbf{e}_p^h = (e_p^h, \bar{e}_p^h, e_{p_f}^h)$, and $\mathbf{e}_p^I = (e_p^I, \bar{e}_p^I, e_{p_f}^I)$.

A standard error estimate of interior penalty discontinuous Galerkin methods (see e.g., [3, 2]) and a discrete Poincaré inequality (cf. [6]) give

$$\|e_{p_f}^I\|_{Q_{h,f}} \leq Ch^s \|p_f\|_{H^{s+1}(\Gamma_c)}, \quad \frac{1}{2} < s \leq k_f, \quad (23a)$$

$$\|e_{p_f}^I\|_{\Gamma_c} \leq Ch^s \|p_f\|_{H^{s+1}(\Gamma_c)}, \quad \frac{1}{2} < s \leq k_f. \quad (23b)$$

If Γ_c is convex, a standard duality argument results in

$$\|e_{p_f}^I\|_{\Gamma_c} \leq Ch^{s+1} \|p_f\|_{H^{s+1}(\Gamma_c)}, \quad \frac{1}{2} < s \leq k_f + 1. \quad (24)$$

Assuming that $(u, p) \in [H^s(\dot{\Omega})]^{\dim} \times H^s(\dot{\Omega})$ for $1 \leq s \leq k+1$, we have by [17, Proposition 3.5] that

$$\|e_p^I\|_{\Omega} \leq Ch^s (\|p\|_{H^s(\dot{\Omega})} + \alpha^{-1} \|\nabla \cdot u\|_{H^{s-1}(\dot{\Omega})}), \quad (25a)$$

$$\|e_u^I\|_{\Omega} \leq Ch^s (\|u\|_{H^s(\dot{\Omega})} + \alpha \|p\|_{H^s(\dot{\Omega})}). \quad (25b)$$

We obtain the error equations in the following lemma.

Lemma 5 (Error equation). *For any $(v_h, \mathbf{q}_h) \in V_h \times \mathbf{Q}_h$ the following system of equations holds:*

$$a_h(e_u^h, v_h) + b_h(v_h, \mathbf{e}_p^h) = \sum_{K \in \mathcal{T}} \int_K \kappa^{-1} e_u^I \cdot v_h \, dx + \sum_{F \in \mathcal{F}_c^I} \int_F e_{p_f}^I [v_h \cdot \mathbf{n}] \, ds, \quad (26a)$$

$$-b_h(e_u^h, \mathbf{q}_h) + c_h(\mathbf{e}_p^h, \mathbf{q}_h) = 0. \quad (26b)$$

Proof. Let (u, p, p_f) be the solution of eqs. (1) and (2) and write $\mathbf{p} = (p, \{\{p\}\}, p_f)$. Furthermore, let (u_h, \mathbf{p}_h) be the solution of eq. (7). Then, by consistency (see lemma 1), we obtain:

$$a_h(u - u_h, v_h) + b_h(v_h, \mathbf{p} - \mathbf{p}_h) = 0 \quad \forall v_h \in V_h, \quad (27a)$$

$$-b_h(u - u_h, \mathbf{q}_h) + c_h(\mathbf{p} - \mathbf{p}_h, \mathbf{q}_h) = 0 \quad \forall \mathbf{q}_h \in \mathbf{Q}_h. \quad (27b)$$

Using the decomposition of the errors introduced in eq. (22),

$$\begin{aligned} a_h(e_u^h, v_h) + b_h(v_h, \mathbf{e}_p^h) &= a_h(e_u^I, v_h) + b_h(v_h, \mathbf{e}_p^I) & \forall v_h \in V_h, \\ -b_h(e_u^h, \mathbf{q}_h) + c_h(\mathbf{e}_p^h, \mathbf{q}_h) &= -b_h(e_u^I, \mathbf{q}_h) + c_h(\mathbf{e}_p^I, \mathbf{q}_h) & \forall \mathbf{q}_h \in \mathbf{Q}_h. \end{aligned}$$

By the definitions of $a_h(\cdot, \cdot)$ in eq. (5a) and $b_h(\cdot, \cdot)$ in eq. (5b), and by properties of the HDG projection eq. (20), we obtain

$$\begin{aligned} a_h(e_u^I, v_h) &= \sum_{K \in \mathcal{T}} \int_K \kappa^{-1} e_u^I \cdot v_h \, dx + \sum_{F \in \mathcal{F}_s^f} \int_F 2\alpha_f^{-1} \{ \{ e_u^I \cdot n \} \} \{ \{ v_h \cdot n \} \} \, ds \\ &\quad + \sum_{F_f \in \mathcal{F}_c^f} \int_F \alpha_f^{-1} \left((\xi - \frac{1}{2}) [[e_u^I \cdot n]] [[v_h \cdot n]] + 2 \{ \{ e_u^I \cdot n \} \} \{ \{ v_h \cdot n \} \} \right) \, ds \\ &= \sum_{K \in \mathcal{T}} \int_K \kappa^{-1} e_u^I \cdot v_h \, dx, \end{aligned}$$

and

$$\begin{aligned} b_h(v_h, e_p^I) &= - \sum_{K \in \mathcal{T}} \int_K e_p^I \nabla \cdot v_h \, dx + \sum_{K \in \mathcal{T}} \int_{\partial K \setminus \Gamma_c} \bar{e}_p^I v_h \cdot n \, ds + \sum_{F \in \mathcal{F}_c^f} \int_F e_{pf}^I [[v_h \cdot n]] \, ds \\ &= \sum_{F \in \mathcal{F}_c^f} \int_F e_{pf}^I [[v_h \cdot n]] \, ds. \end{aligned}$$

These identities complete the proof of eq. (26a).

For eq. (26b), note that integration by parts gives

$$\begin{aligned} -b_h(e_u^I, \mathbf{q}_h) &= \sum_{K \in \mathcal{T}} \int_K q_h \nabla \cdot e_u^I \, dx - \sum_{K \in \mathcal{T}} \int_{\partial K \setminus \Gamma_c} \bar{q}_h e_u^I \cdot n \, ds - \sum_{F_f \in \mathcal{F}_c^f} \int_F q_{h,f} [[e_u^I \cdot n]] \, ds \\ &= - \sum_{K \in \mathcal{T}} \int_K \nabla q_h \cdot e_u^I \, dx + \sum_{K \in \mathcal{T}} \int_{\partial K \setminus \Gamma_c} (q_h - \bar{q}_h) e_u^I \cdot n \, ds - \sum_{F \in \mathcal{F}_c^f} \int_F q_{h,f} [[e_u^I \cdot n]] \, ds \\ &\quad + \sum_{K \in \mathcal{T}} \int_{\partial K \cap \Gamma_c} q_h e_u^I \cdot n \, ds \\ &= \sum_{K \in \mathcal{T}} \int_{\partial K \setminus \Gamma_c} (q_h - \bar{q}_h) e_u^I \cdot n \, ds - \sum_{F \in \mathcal{F}_c^f} \int_F q_{h,f} [[e_u^I \cdot n]] \, ds + \sum_{K \in \mathcal{T}} \int_{\partial K \cap F, F \in \mathcal{F}_c^f} q_h e_u^I \cdot n \, ds \\ &= \sum_{K \in \mathcal{T}} \int_{\partial K \setminus \Gamma_c} (q_h - \bar{q}_h) e_u^I \cdot n \, ds \\ &= \sum_{K \in \mathcal{T}} \int_{\partial K \setminus (\Gamma_c \cup \Gamma_s)} (q_h - \bar{q}_h) e_u^I \cdot n \, ds, \end{aligned}$$

where the last two equalities are because of eq. (20c). Furthermore, by definition of $c_h(\cdot, \cdot)$ in eq. (5d), eq. (21), and the definition of $\bar{\Pi}_Q$,

$$\begin{aligned} c_h(e_p^I, \mathbf{q}_h) &= c_h^f(e_{pf}^I, q_{h,f}) + \sum_{K \in \mathcal{T}} \int_{\partial K \setminus (\Gamma_c \cup \Gamma_s)} \alpha(e_p^I - \bar{e}_p^I) (q_h - \bar{q}_h) \, ds \\ &= \sum_{K \in \mathcal{T}} \int_{\partial K \setminus (\Gamma_c \cup \Gamma_s)} \alpha(e_p^I - \bar{e}_p^I) (q_h - \bar{q}_h) \, ds \\ &= \sum_{K \in \mathcal{T}} \int_{\partial K \setminus (\Gamma_c \cup \Gamma_s)} \alpha e_p^I (q_h - \bar{q}_h) \, ds. \end{aligned} \tag{28}$$

By eq. (20c) we find $-b_h(e_u^I, \mathbf{q}_h) + c_h(e_p^I, \mathbf{q}_h) = 0$, which completes the proof of eq. (26b). \square

Theorem 2. Suppose that $u \in [H^s(\dot{\Omega})]^{\dim}$, $p \in H^s(\dot{\Omega})$, $1 \leq s \leq k+1$ and $p_f \in H^{s_f+1}(\Gamma_c)$ for $\frac{1}{2} < s_f \leq k_f$. Then,

$$\|u - u_h\|_{\Omega} + \|p_f - p_{f,h}\|_{Q_{h,f}} \leq C\kappa_{\min}^{-1} h^s (\|u\|_{H^s(\dot{\Omega})} + \|p\|_{H^s(\dot{\Omega})}) + Ch^{s_f} \|p_f\|_{H^{s_f+1}(\Gamma_c)}, \quad (29)$$

with $C > 0$ depending on a discrete trace inequality constant, the penalty parameter σ , and the parameters κ_{\min} , α_f^{-1} , and ξ , and

$$\|p - p_h\|_{\Omega} \leq C_1 h^s (\|u\|_{H^s(\dot{\Omega})} + \|p\|_{H^s(\dot{\Omega})}) + C_2 h^{s_f} \|p_f\|_{H^{s_f+1}(\Gamma_c)}, \quad (30)$$

where $C_1, C_2 > 0$ depend on κ_{\min} , α_f^{-1} , and ξ .

Moreover, if eq. (24) holds, then h^{s_f} in the above estimates can be replaced by h^{s_f+1} .

Proof. Taking $v_h = e_u^h$, $\mathbf{q}_h = \mathbf{e}_p^h$ in eq. (26), adding eqs. (26a) and (26b), and using the Cauchy–Schwarz inequality, we obtain:

$$a_h(e_u^h, e_u^h) + c_h(\mathbf{e}_p^h, \mathbf{e}_p^h) \leq \left(\kappa_{\min}^{-1} \|e_u^I\|_{\Omega} + \|e_{p_f}^I\|_{\Gamma_c} \right) \|e_u^h\|_{V_h}. \quad (31)$$

Using the coercivity of a_h (see eq. (13a)) and the positive semi-definiteness of c_h (see lemma 3), we obtain:

$$a_h(e_u^h, e_u^h) + c_h(\mathbf{e}_p^h, \mathbf{e}_p^h) \geq C_c (\|e_u^h\|_{V_h}^2 + \|e_{p_f}^h\|_{Q_{h,f}}^2) + \alpha \sum_{K \in \mathcal{T}} \|e_p^h - \bar{e}_p^h\|_{\partial K \setminus (\Gamma_c \cup \Gamma_s)}^2, \quad (32)$$

with $C_c = \min \{ \kappa_{\max}^{-1}, \alpha_f^{-1}(\xi - 1/2), C\kappa_{\min} \}$. Applying Young's inequality to the right hand side of eq. (31) and combining eqs. (31) and (32), we obtain:

$$\frac{1}{2} C_c \|e_u^h\|_{V_h}^2 + C_c \|e_{p_f}^h\|_{Q_{h,f}}^2 + \alpha \sum_{K \in \mathcal{T}} \|e_p^h - \bar{e}_p^h\|_{\partial K \setminus (\Gamma_c \cup \Gamma_s)}^2 \leq \frac{1}{2} C_c^{-1} \left(\kappa_{\min}^{-1} \|e_u^I\|_{\Omega} + \|e_{p_f}^I\|_{\Gamma_c} \right)^2. \quad (33)$$

Equation (29) follows by a triangle inequality, eqs. (23b) and (25b).

We next prove eq. (30). It is known (cf. [19] and [4, Lemma B.1]) that there exists $w \in [H^1(\Omega)]^{\dim}$ such that $\nabla \cdot w = -e_p^h$ and $\|w\|_{H^1(\Omega)} \leq C \|e_p^h\|_{\Omega}$ with $C > 0$ only depending on Ω . Then,

$$\|e_p^h\|_{\Omega}^2 = - \int_{\Omega} e_p^h \nabla \cdot w \, dx = \int_{\Omega} \nabla e_p^h \cdot w \, dx - \sum_{K \in \mathcal{T}} \int_{\partial K} e_p^h w \cdot n \, ds.$$

For every $K \in \mathcal{T}$, we fix a face $F \in \mathcal{F}_0$ of K and define $\tilde{\Pi}_K^F$ using eq. (14). Then we introduce $\tilde{\Pi} : [H^1(\Omega)]^{\dim} \rightarrow V_h$ such that $\tilde{\Pi}w = \tilde{\Pi}_K^F w$ on each K . By eq. (14a), $\int_{\Omega} \nabla e_p^h \cdot w \, dx = \int_{\Omega} \nabla e_p^h \cdot \tilde{\Pi}w \, dx$. Applying this to the above identity,

$$\begin{aligned} \|e_p^h\|_{\Omega}^2 &= \int_{\Omega} \nabla e_p^h \cdot \tilde{\Pi}w \, dx - \sum_{K \in \mathcal{T}} \int_{\partial K} e_p^h w \cdot n \, ds \\ &= \int_{\Omega} \nabla e_p^h \cdot \tilde{\Pi}w \, dx + \sum_{K \in \mathcal{T}} \int_{\partial K \setminus (\Gamma_c \cup \Gamma_s)} (\bar{e}_p^h - e_p^h) w \cdot n \, ds \\ &\quad - \sum_{K \in \mathcal{T}} \int_{\partial K \cap (\Gamma_c \cup \Gamma_s)} e_p^h w \cdot n \, ds, \end{aligned} \quad (34)$$

where for the second equality we used the normal continuity of $w \cdot n$ on $F \in \mathcal{F}_0 \cup \mathcal{F}_s^f$, single-valuedness of \bar{e}_p^h , and that $\bar{e}_p^h = 0$ on $F \in \mathcal{F}_b$. Using integration by parts we note that

$$\begin{aligned} b_h(\tilde{\Pi}w, \mathbf{e}_p^h) &= \int_{\Omega} \nabla e_p^h \cdot \tilde{\Pi}w \, dx + \sum_{K \in \mathcal{T}} \int_{\partial K \setminus (\Gamma_c \cup \Gamma_s)} (\bar{e}_p^h - e_p^h) \tilde{\Pi}w \cdot n \, ds \\ &\quad - \sum_{K \in \mathcal{T}} \int_{\partial K \cap (\Gamma_c \cup \Gamma_s)} e_p^h \tilde{\Pi}w \cdot n \, ds + \sum_{F \in \mathcal{F}_c^f} \int_F e_{p_f}^h [[\tilde{\Pi}w \cdot n]] \, ds. \end{aligned} \quad (35)$$

Combining eqs. (34) and (35),

$$\begin{aligned} \|e_p^h\|_\Omega^2 &= b_h(\tilde{\Pi}w, e_p^h) + \sum_{K \in \mathcal{T}} \int_{\partial K \setminus (\Gamma_c \cup \Gamma_s)} (\bar{e}_p^h - e_p^h)(w - \tilde{\Pi}w) \cdot n \, ds \\ &\quad - \sum_{K \in \mathcal{T}} \int_{\partial K \cap (\Gamma_c \cup \Gamma_s)} e_p^h(w - \tilde{\Pi}w) \cdot n \, ds - \sum_{F \in \mathcal{F}_c^f} \int_F e_{p_f}^h [\tilde{\Pi}w \cdot n] \, ds. \end{aligned}$$

Since $w \cdot n$ is continuous on Γ_c and $\tilde{\Pi}w \cdot n|_F = P_F w \cdot n|_F$ for $F \in \mathcal{F}_c^f \cup \mathcal{F}_s^f$,

$$\|e_p^h\|_\Omega^2 = b_h(\tilde{\Pi}w, e_p^h) + \sum_{K \in \mathcal{T}} \int_{\partial K \setminus (\Gamma_c \cup \Gamma_s)} (\bar{e}_p^h - e_p^h)(w - \tilde{\Pi}w) \cdot n \, ds. \quad (36)$$

Let $P_{\partial K} w \cdot n$ be the face-wise L^2 -orthogonal projection of $w \cdot n$ into $P_k(\partial K)$. Taking $v_h = \tilde{\Pi}w$ in eq. (26a), combining with eq. (36), using the L^2 -orthogonality of $w \cdot n - P_{\partial K} w \cdot n$ to $P_k(\partial K)$, and the continuity of $\tilde{\Pi}w \cdot n$ on $\Gamma_c \cup \Gamma_s$, we obtain:

$$\begin{aligned} \|e_p^h\|_\Omega^2 &= \sum_{K \in \mathcal{T}} \int_{\partial K \setminus (\Gamma_c \cup \Gamma_s)} (\bar{e}_p^h - e_p^h)(P_{\partial K} w \cdot n - \tilde{\Pi}w \cdot n) \, ds - a_h(e_u^h, \tilde{\Pi}w) \\ &\quad + \sum_{K \in \mathcal{T}} \int_K \kappa^{-1} e_u^I \cdot \tilde{\Pi}w \, dx \\ &=: I_1 + I_2 + I_3. \end{aligned} \quad (37)$$

By the Cauchy–Schwarz inequality and eq. (15a),

$$|I_1| \leq Ch^{\frac{1}{2}} \left(\sum_{K \in \mathcal{T}} \|e_p^h - \bar{e}_p^h\|_{\partial K \setminus (\Gamma_c \cup \Gamma_s)}^2 \right)^{\frac{1}{2}} \|e_p^h\|_\Omega.$$

We next bound I_2 . By eq. (13b),

$$|I_2| \leq C \max\{\kappa_{\min}^{-1}, \alpha_f^{-1}\} \|e_u^h\|_{V_h} \|\tilde{\Pi}w\|_{V_h}. \quad (38)$$

Using that $\tilde{\Pi}w \cdot n$ is continuous on Γ_c in the definition of $\|\cdot\|_{V_h}$:

$$\|\tilde{\Pi}w\|_{V_h}^2 = \|\tilde{\Pi}w\|_\Omega^2 + \sum_{F \in \mathcal{F}_c^f} \|\{\tilde{\Pi}w \cdot n\}\|_F^2 + \sum_{F \in \mathcal{F}_s^f} \|\{\tilde{\Pi}w \cdot n\}\|_F^2. \quad (39)$$

By the trace inequality $\|w\|_{H^{1/2}(\Gamma_c \cup \Gamma_s)} \leq C \|w\|_{H^1(\Omega)}$ we find

$$\|\{\tilde{\Pi}w \cdot n\}\|_{\Gamma_c \cup \Gamma_s} \leq \|w \cdot n\|_{\Gamma_c \cup \Gamma_s} \leq C \|w\|_{H^1(\Omega)} \leq C \|e_p^h\|_\Omega. \quad (40)$$

Furthermore, by eq. (15b), we note that

$$\|\tilde{\Pi}w\|_K \leq \|\tilde{\Pi}w - w\|_K + \|w\|_K \leq Ch_K \|w\|_{H^1(K)} + \|w\|_K \leq C \|w\|_{H^1(K)},$$

and so $\|\tilde{\Pi}w\|_\Omega \leq C \|w\|_{H^1(\Omega)} \leq C \|e_p^h\|_\Omega$. Using this inequality and eq. (40) in eq. (39) we find that $\|\tilde{\Pi}w\|_{V_h}^2 \leq C \|e_p^h\|_\Omega^2$. Therefore, in combination with eq. (38),

$$|I_2| \leq C \max\{\kappa_{\min}^{-1}, \alpha_f^{-1}\} \|e_u^h\|_{V_h} \|e_p^h\|_\Omega,$$

and by the Cauchy–Schwarz inequality, $|I_3| \leq C \kappa_{\min}^{-1} \|e_u^I\|_\Omega \|e_p^h\|_\Omega$. Combining eq. (37) with the bounds for I_1, I_2, I_3 , and using Young’s inequality,

$$\|e_p^h\|_\Omega^2 \leq Ch \sum_{K \in \mathcal{T}} \|e_p^h - \bar{e}_p^h\|_{\partial K \setminus (\Gamma_c \cup \Gamma_s)}^2 + C(\max\{\kappa_{\min}^{-1}, \alpha_f^{-1}\})^2 \|e_u^h\|_{V_h}^2 + C \kappa_{\min}^{-2} \|e_u^I\|_\Omega^2.$$

Applying eq. (33),

$$\begin{aligned} \|e_p^h\|_\Omega^2 &\leq \left[Ch\alpha^{-1}C_c^{-1} + C(\max\{\kappa_{\min}^{-1}, \alpha_f^{-1}\})^2 C_c^{-2} \right] \left(\kappa_{\min}^{-1} \|e_u^I\|_\Omega + \|e_{p_f}^I\|_{\Gamma_c} \right)^2 \\ &\quad + C\kappa_{\min}^{-2} \|e_u^I\|_\Omega^2. \end{aligned}$$

Equation (30) now follows by the triangle inequality, eqs. (23b), (25a) and (25b). \square

Remark 2. *The error estimates eqs. (29) and (30) show that if $s = k + 1$ and $s_f = k_f$, then the errors in the velocity and pressures in the L^2 -norm are $\mathcal{O}(h^{\min(k+1, k_f+1)})$ if the duality argument eq. (24) holds on the fault, and $\mathcal{O}(h^{\min(k+1, k_f)})$ otherwise. Hence, if the duality argument holds it suffices to choose $k_f = k$ in Q_h^f to obtain errors of $\mathcal{O}(h^{k+1})$. If the duality argument does not hold, then errors of $\mathcal{O}(h^{k+1})$ can be obtained by choosing $k_f = k + 1$.*

6 Numerical results

We showcase the performance of the proposed HDG/DG scheme in various examples below¹. In section 6.1 we verify the convergence properties of the discretization established in theorem 2. Afterwards, in sections 6.2 to 6.4, we apply the HDG/DG method to various benchmark problems to demonstrate its robustness in different scenarios, including whether the fault is conducting or sealing, whether it is fully, partially, or not immersed, and whether there are multiple faults that may or may not intersect. All the examples were implemented using the FEniCS [26]-based library FEniCSii [21] for coupled inter-dimensional problems.

6.1 Error convergence

We consider a domain $\Omega = (-1, 1)^2$ split into subdomains $\Omega_1, \Omega_2, \Omega_3$ by a pair of vertical faults; a conducting fault Γ_c given by the line segment that connects points $[-0.5, -1]$ and $[-0.5, 1]$ and a sealing fault Γ_s defined by points $[0.5, -1]$ and $[0.5, 1]$. For the exact solution, we choose p and p_f as follows

$$p = \begin{cases} \sin(\pi(x + y)) & [x, y] \in \Omega_1 \\ \cos(\pi(x + y)) & [x, y] \in \Omega_2, \quad p_f = \sin(\pi(x - 2y)) \\ \cos(\pi(2x - y)) & [x, y] \in \Omega_3 \end{cases}$$

and adjust the right-hand sides of eqs. (1d) to (1g) accordingly. We prescribe p and p_f as boundary data on the top and bottom edges of Ω and $\partial\Gamma_c = (\partial\Gamma_c)^D$, respectively. The corresponding normal flux $u \cdot n$ is set on the lateral edges. A sample mesh used in the (uniform) refinement study is shown in fig. 2. In the experiments we let $\alpha_f = 2$, $\xi = 0.75$, $\kappa_f = 3$ and consider a discontinuous permeability κ such that $\kappa|_{\Omega_1} = 5$, $\kappa|_{\Omega_2} = 4$ and $\kappa|_{\Omega_3} = 6$. The stabilization parameter is set as $\sigma = 10k^2$.

Errors in u , p , and p_f in the L^2 -norm are shown for different levels of refinement and for $k = 1, 2, 3$, $k_f = k$ in table 1 together with rates of convergence. We observe that the errors for all the unknowns approach the order $\mathcal{O}(h^{k+1})$, as expected from theorem 2.

Remark 3 (Non-convex Γ_c). *In the previous example the convexity of Γ_c ensured that the estimate (24) held and in turn, following theorem 2, taking $k_f = k$ was sufficient to achieve convergence order $k + 1$. Here we consider a setup where Γ_c is not convex and the duality argument may not hold.*

We let $\Omega = (-1, 1) \times (-0.5, 1.5)$ and split the domain into Ω_+, Ω_- by a single conducting fracture Γ_c defined as a union of three segments $\Gamma_{c,1}, \Gamma_{c,2}$ and $\Gamma_{c,3}$, cf. fig. 3. We define the exact solution p and p_f as

¹Further numerical experiments using two alternative hybridizable discretizations based on a similar philosophy as the HDG/DG scheme, where the inter-dimensional coupling between the problems is naturally handled by the face variables, are presented in A without analysis.

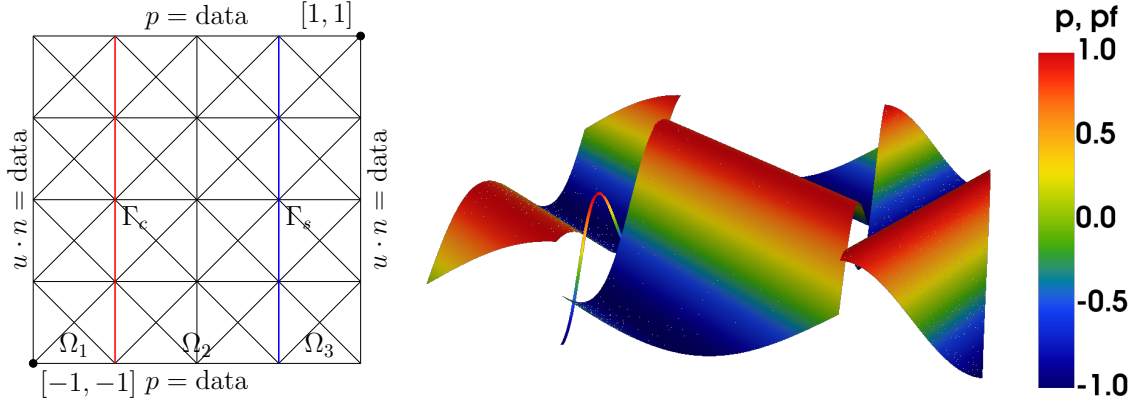


Figure 2: Setup of the error convergence study in section 6.1. (Left) Geometry with a conducting fault in red, sealing fault in blue, and a sample mesh. (Right) Discrete pressures on the finest mesh ($h = 1/64$) with the HDG/DG discretization choosing $k = k_f = 1$.

h	$\ u - u_h\ _{\Omega}$	$\ p - p_h\ _{\Omega}$	$\ p_f - p_{h,f}\ _{\Gamma_c}$
$k = 1$			
0.5	6.984E+00(-)	8.934E-01(-)	2.026E-01(-)
0.25	1.842E+00(1.92)	2.010E-01(2.15)	1.943E-01(0.06)
0.125	4.654E-01(1.98)	4.715E-02(2.09)	5.082E-02(1.93)
0.0625	1.165E-01(2.00)	1.129E-02(2.06)	1.309E-02(1.96)
0.0312	2.909E-02(2.00)	2.754E-03(2.04)	3.323E-03(1.98)
0.0156	7.267E-03(2.00)	6.795E-04(2.02)	8.371E-04(1.99)
$k = 2$			
0.5	1.470E+00(-)	1.522E-01(-)	1.992E-01(-)
0.25	1.888E-01(2.96)	2.001E-02(2.93)	2.105E-02(3.24)
0.125	2.366E-02(3.00)	2.373E-03(3.08)	2.759E-03(2.93)
0.0625	2.950E-03(3.00)	2.863E-04(3.05)	3.484E-04(2.99)
0.0312	3.680E-04(3.00)	3.508E-05(3.03)	4.365E-05(3.00)
0.0156	4.594E-05(3.00)	4.338E-06(3.02)	5.459E-06(3.00)
$k = 3$			
0.5	2.385E-01(-)	2.981E-02(-)	6.027E-03(-)
0.25	1.573E-02(3.92)	1.624E-03(4.20)	1.923E-03(1.65)
0.125	9.905E-04(3.99)	9.712E-05(4.06)	1.238E-04(3.96)
0.0625	6.190E-05(4.00)	5.893E-06(4.04)	7.829E-06(3.98)
0.0312	3.864E-06(4.00)	3.622E-07(4.02)	4.916E-07(3.99)
0.0156	2.413E-07(4.00)	2.244E-08(4.01)	3.079E-08(4.00)

Table 1: Convergence of the HDG/DG approximation with $k_f = k = 1, 2, 3$ to the solution of the coupled problem setup in section 6.1. Errors are reported in the L^2 -norms on the respective domains. Estimated rates are shown in the brackets.

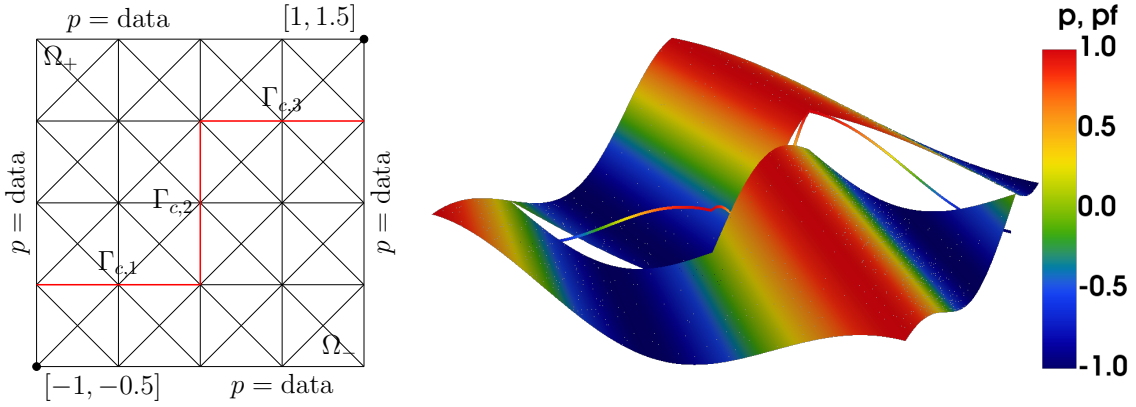


Figure 3: Setup of the error convergence study in remark 3. (Left) Geometry with a non-convex conducting fault in red, and a sample mesh. (Right) Discrete pressures on the finest mesh ($h = 1/64$) with the HDG/DG discretization choosing $k = k_f = 1$.

follows

$$p|_{\Omega_+} = \sin(\pi(x+y)), \quad p|_{\Omega_-} = \cos(\pi(x/2+y)), \quad p_f = \begin{cases} \cos(2\pi y) & [x, y] \in \Gamma_{c,2} \\ \cos(\pi x) & [x, y] \in \Gamma_{c,1} \cup \Gamma_{c,3} \end{cases}.$$

We prescribe p and p_f as boundary data on $\partial\Omega$ and $\partial\Gamma_c = (\partial\Gamma_c)^D$, respectively and set the model parameters as $\alpha_f = 2$, $\xi = 0.75$, $\kappa_f = 3$ while considering a discontinuous permeability κ such that $\kappa|_{\Omega_+} = 5$, $\kappa|_{\Omega_-} = 4$. Accordingly we also adjust the right-hand sides of eqs. (1d) and (1e).

Setting $k_f = k$, $k = 1, 2, 3$ and (as before) $\sigma = 10k^2$ we observe in table 2 that while Γ_c is non-convex, the HDG/DG scheme still yields convergence rates of order $k+1$ for u , p and p_f without the need to choose $k_f = k+1$.

6.2 Conducting faults

To illustrate the flexibility of modeling the conducting faults through eqs. (1c) to (1e) we consider two model problems with $\Omega = (0, 1)^2$ having bulk permeability $\kappa = 1$ and which includes a single fracture characterized by $g_f = 1$ and $0.5 < \xi \leq 1$.

In the first problem the domain contains an embedded fault extending from $[0.25, 0.75]$ to $[0.75, 0.25]$ with thickness $d = 10^{-3}$ and $\bar{\kappa}_{f,\tau} = \bar{\kappa}_{f,n} = 10^8$ (see [25]). Boundary conditions are depicted in fig. 4. The authors in [25] do not apply eqs. (1c) to (1e) on the fracture. Instead, they model the conducting fault by eq. (1c) and the pressure continuity condition $p_+ = p_- = p_f$ on Γ_c , see also [1]. As noted in [27], eqs. (1c) to (1e) allow for pressure discontinuity on the fracture and the continuity conditions $p_+ = p_- = p_f$ correspond to the limit case $\alpha_f = +\infty$ in eqs. (1d) and (1e) where fracture permeability is assumed to be large and the thickness of the fracture is assumed to be small. Therefore, since $\alpha_f = 2 \times 10^{11}$, for the reference solutions, we use continuous linear Lagrange elements (P_1) that enforce the above mentioned pressure continuity conditions by construction of the finite element space. In fig. 4 we compare the HDG/DG solutions to this reference P_1 solution by sampling the pressure along the predefined line $y = 0.5$ that crosses the fault. We observe that the results of the HDG/DG method match well with the results of the conforming scheme.

In the second problem, inspired by [27], the domain is split by a vertical fracture with $d = 10^{-2}$ and a discontinuous fracture permeability with $\bar{\kappa}_{f,\tau} = \bar{\kappa}_{f,n} = 1$ on segments AB and CD and $\bar{\kappa}_{f,\tau} = \bar{\kappa}_{f,n} = 2 \cdot 10^{-3}$ in the middle part BC . Figure 5 shows this domain together with boundary conditions. We use the mixed finite element discretization proposed in [27] that uses the lowest order Raviart–Thomas elements paired with piecewise constant pressures to obtain a reference solution. In fig. 5 we compare the HDG/DG solutions to the reference solution. As before, we sample the pressure along a predefined line that crosses the fault. The results are in very good agreement with [27]. This shows that our method can handle different values of

h	$\ u - u_h\ _{\Omega}$	$\ p - p_h\ _{\Omega}$	$\ p_f - p_{h,f}\ _{\Gamma_c}$
$k = 1$			
0.5	2.288E+00(-)	2.779E-01(-)	2.269E-01(-)
0.25	6.244E-01(1.87)	6.419E-02(2.11)	1.544E-01(0.56)
0.125	1.600E-01(1.96)	1.510E-02(2.09)	4.020E-02(1.94)
0.0625	4.030E-02(1.99)	3.639E-03(2.05)	9.959E-03(2.01)
0.0312	1.010E-02(2.00)	8.916E-04(2.03)	2.497E-03(2.00)
0.0156	2.526E-03(2.00)	2.206E-04(2.02)	6.252E-04(2.00)
$k = 2$			
0.5	3.617E-01(-)	3.519E-02(-)	1.483E-01(-)
0.25	3.885E-02(3.22)	3.990E-03(3.14)	1.538E-02(3.27)
0.125	4.656E-03(3.06)	4.685E-04(3.09)	1.973E-03(2.96)
0.0625	5.704E-04(3.03)	5.647E-05(3.05)	2.505E-04(2.98)
0.0312	7.065E-05(3.01)	6.921E-06(3.03)	3.136E-05(3.00)
0.0156	8.793E-06(3.01)	8.564E-07(3.01)	3.921E-06(3.00)
$k = 3$			
0.5	2.748E-02(-)	3.359E-03(-)	4.758E-03(-)
0.25	2.019E-03(3.77)	1.916E-04(4.13)	1.384E-03(1.78)
0.125	1.191E-04(4.08)	1.124E-05(4.09)	8.906E-05(3.96)
0.0625	7.086E-06(4.07)	6.773E-07(4.05)	5.588E-06(3.99)
0.0312	4.296E-07(4.04)	4.151E-08(4.03)	3.500E-07(4.00)
0.0156	2.640E-08(4.02)	2.568E-09(4.01)	2.189E-08(4.00)

Table 2: Convergence of the HDG/DG approximation with $k_f = k = 1, 2, 3$ to the solution of the coupled problem setup in remark 3 with non-convex conducting fracture. Errors are reported in the L^2 -norms on the respective domains. Estimated rates are shown in the brackets.

α_f , including the limit case. We note that in both test problems the results of the HDG/DG scheme show little sensitivity to the choice of parameter ξ . In the following test cases of conducting faults we therefore set $\xi = 0.75$.

6.3 Sealing faults

We next consider sealing faults. We consider the domain $\Omega = (0, 1)^2$ which includes either a single partially immersed sealing fault extending from $[0.5, 1]$ to $[0.5, 0.5]$ or a fully immersed sealing fault from $[0.25, 0.75]$ to $[0.75, 0.25]$. We set the bulk permeability as $\kappa = 1$, the fault thickness as $d = 10^{-3}$, and $\bar{\kappa}_{f,n} = 10^{-8}$. We prescribe a pressure gradient in the horizontal direction by setting $p = 0$ on the left boundary and $p = 1$ on the right boundary. On the bottom and top boundaries we impose $u \cdot n = 0$. See the left and center panels in figs. 6 and 7 for the problem setup and pressure solution, respectively.

As in section 6.2 will compare the pressure solution obtained with the HDG/DG method ($k = k_f = 1$) to a reference solution obtained with a conforming scheme and on a finer mesh. For the conforming scheme, however, we now consider a mixed discretization [22] using the RT_0 - P_0 elements. This discretization enforces flux conservation on Γ_s by construction. As before the comparison is made by sampling the pressure along a predefined line that crosses the fault. From the right most panels in figs. 6 and 7 we once again observe a good match of the pressure values and that the results are in good agreement with the results from [25].

6.4 Intersecting faults

In this final numerical examples section we consider three benchmark problems from [18]:

1. The hydrocoin problem. For this problem the domain is depicted in fig. 8. The domain contains two intersecting conducting faults with permeability $\bar{\kappa}_{f,\tau} = \bar{\kappa}_{f,n} = 10^{-6}$. The width of the AB fault is $d = 5\sqrt{2}$ and the width of the second fault is $d = 33/\sqrt{5}$. The surrounding medium has permeability $\kappa = 10^{-8}$.
2. The regular fault network problem. For this problem, $\kappa = 1$ and the domain includes axis-aligned conducting faults with width $d = 10^{-4}$ and $\bar{\kappa}_{f,\tau} = \bar{\kappa}_{f,n} = 10^4$. See fig. 9.

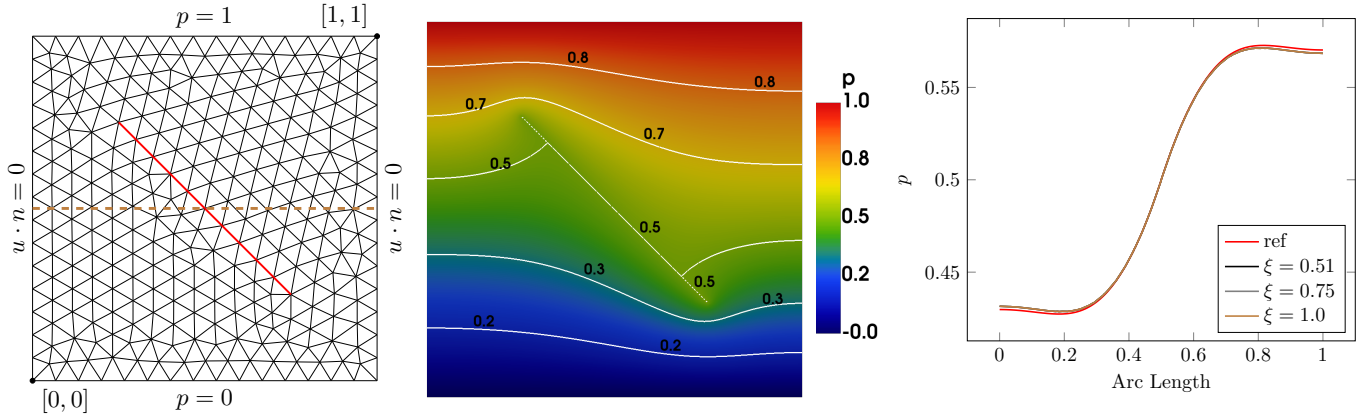


Figure 4: Fully immersed conducting fault problem described in section 6.2. (Left) Problem setup together with the initial mesh. The conducting fault is depicted by a red line. To compare solutions of different discretizations we sample the pressure along the brown dashed line. (Center) The pressure distribution obtained by the HDG/DG method with $\xi = 0.75$. (Right) Comparison of HDG/DG solutions for three different values of ξ to a reference P_1 solution of the fracture model [1] in terms of pressure values sampled along the brown dashed line in the left panel. The conforming scheme reflects the modeling assumption $p_+ = p_- = p_f$ on Γ_c [1]. Note that no value of ξ is needed for the reference solution. The HDG/DG solution was computed on a coarse mesh with 2176 cells while a fine mesh consisting of 30056 cells is used to compute the P_1 reference solution.

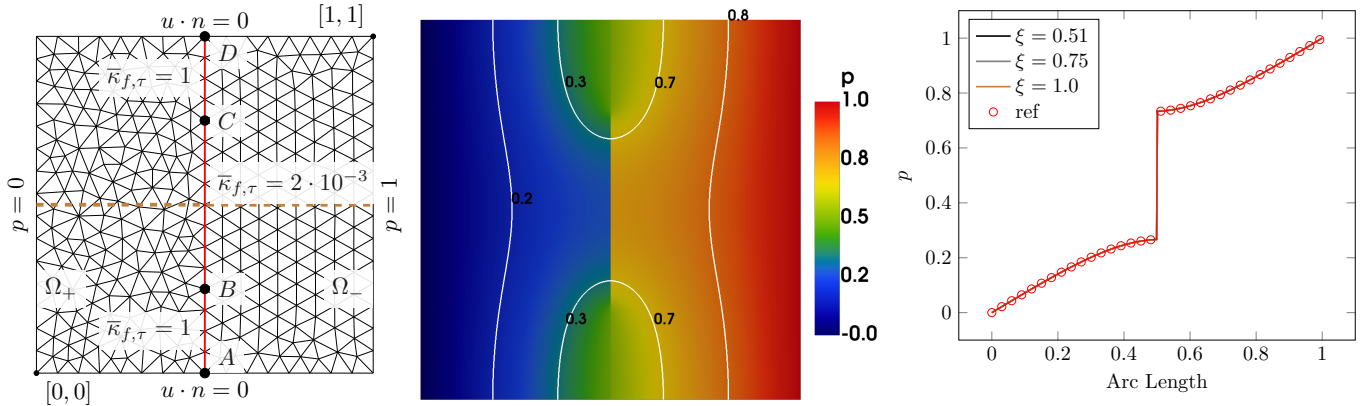


Figure 5: Conducting fault with discontinuous permeability $\bar{\kappa}_{f,n} = \bar{\kappa}_{f,\tau}$ as described in section 6.2. (Left) Problem setup together with the initial mesh. The conducting fault is depicted by a red line. To compare solutions of different discretizations we sample the pressure along the brown dashed line. (Center) The pressure distribution obtained by the HDG/DG method with $\xi = 0.75$. (Right) Comparison of HDG/DG solutions for three different values of ξ to a reference RT_0 - P_0 solution [27] where $\xi = 1$ in terms of pressure values sampled along the brown dashed line in the left panel. The HDG/DG solution was computed on a coarse mesh with 2286 cells while a fine mesh with 32354 cells was used for the reference solution. For clarity, the reference solution is shown as a thin red line as well as using markers.

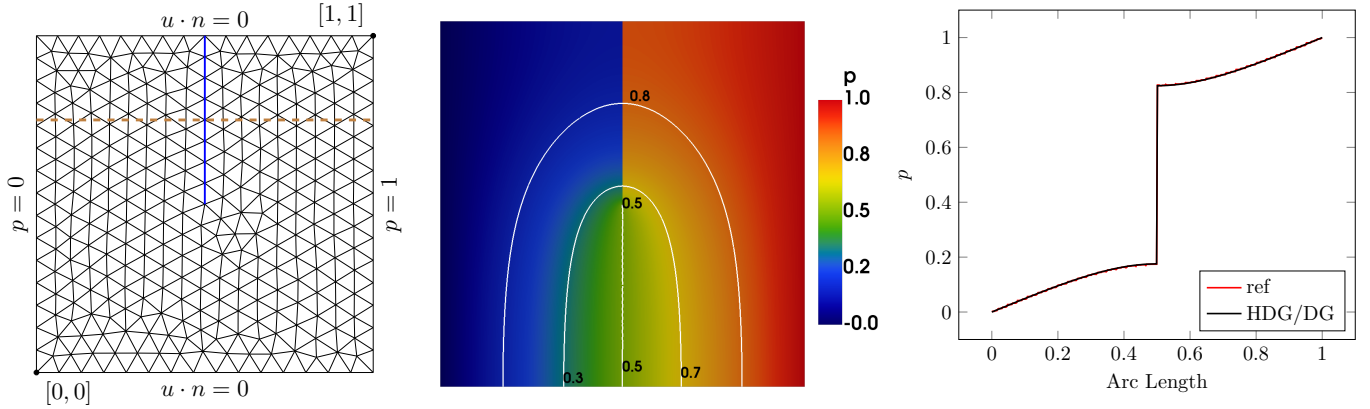


Figure 6: Partially immersed sealing fault problem as described in section 6.3. (Left) Problem setup together with the initial mesh. The sealing fault is depicted by a blue line. To compare solutions of different discretizations we sample the pressure along the brown dashed line. (Center) The pressure distribution obtained by the HDG/DG method. (Right) Comparison of HDG/DG to the RT_0 - P_0 reference solution in terms of pressure values sampled along the brown dashed line in the left panel. The HDG/DG solution was computed on a coarse mesh consisting of 2037 cells while a fine mesh consisting of 7703 cells is used to compute the RT_0 - P_0 reference solution.

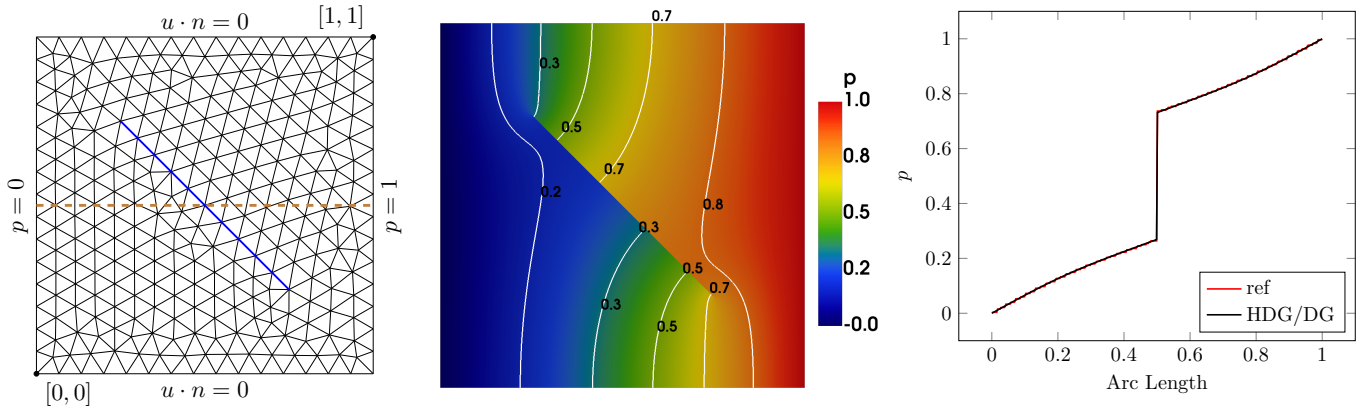


Figure 7: Fully immersed sealing fault problem as described in section 6.3. (Left) Problem setup together with the initial mesh. The sealing fault is depicted by a blue line. To compare solutions of different discretizations we sample the pressure along the brown dashed line. (Center) The pressure distribution obtained by the HDG/DG method. (Right) Comparison of HDG/DG to the RT_0 - P_0 reference solution in terms of pressure values sampled along the brown dashed line in the left panel. The HDG/DG solution was computed on a coarse mesh consisting of 1950 cells while a fine mesh consisting of 7580 cells is used to compute the RT_0 - P_0 reference solution.

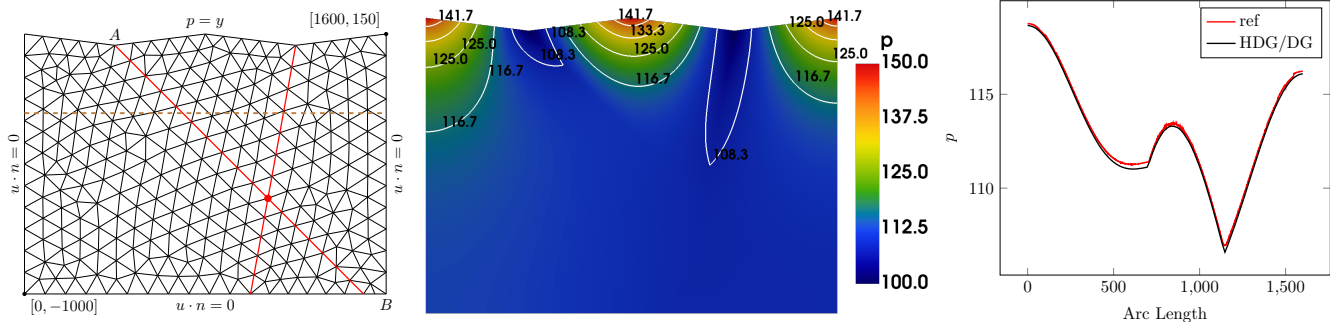


Figure 8: The hydrocoin problem as described in section 6.4. (Left) Problem setup together with the initial mesh. Conducting faults are depicted by red lines. To compare solutions of different discretizations we sample the pressure along the brown dashed line. (Center) The pressure distribution obtained by the HDG/DG method. (Right) Comparison of the HDG/DG pressure solution computed on a mesh with 7705 cells to the reference pressure solution computed using MFD on a mesh with approximately 42500 (mixed - quadrilateral/triangular) cells [18].

3. The complex fault network problem. This problem includes eight conducting faults with $\bar{\kappa}_{f,\tau} = \bar{\kappa}_{f,n} = 10^4$ and two sealing faults with $\bar{\kappa}_{f,n} = 10^{-4}$, see fig. 10. The width of all faults is $d = 10^{-4}$ and we set $\kappa = 1$ in the bulk.

In all the examples when modeling the conducting faults we set $\xi = 0.75$ in eqs. (1d) and (1e), cf. section 6.2, and set $g_f = 0$. The boundary conditions for each of the benchmark problems are specified in the left most panels of figs. 8 to 10.

As in sections 6.2 and 6.3 the comparison of solutions of the HDG/DG discretization against the reference solutions is done in terms of pressure solutions along predefined lines crossing (some of) the faults. For the HDG/DG methods we choose $k = k_f = 1$ and relatively coarse meshes (7705 cells for the hydrocoin problem, 2382 cells for the regular fault network problem, and 2744 cells for the complex fault network problem). We use a mimetic finite difference (MFD) method [8], on much finer meshes, to compute the reference solution because this is the method used to obtain the results in [18].

In all three problems the HDG/DG pressure solution agrees well with the reference pressure solution obtained with the MFD method. The solution profiles also match well with those given in [18].

7 Conclusions

Due to the introduction of (dim - 1)-dimensional face unknowns, the HDG discretization provides a natural framework to couple dim-dimensional problems to (dim - 1)-dimensional problems. We exploit this to introduce a discretization for porous media with faults in which we discretize the dim-dimensional Darcy equations by an HDG method and the (dim - 1)-dimensional fault problem by an IPDG method. We proved the well-posedness of this discretization and presented an a priori error analysis. Manufactured solution numerical examples verify our analysis while benchmark problems show good comparison of the HDG/DG solution with solutions obtained with other discretizations. Future work includes the design of iterative solvers specifically for the hybridized form of the proposed HDG/DG discretization.

Acknowledgments

AC and JJL are supported by the National Science Foundation under Grant No. DMS-2110782 and DMS-2110781, respectively. MK acknowledges funding from the Research Council of Norway (grant no. 303362) and SR was funded by a Discovery Grant from the Natural Sciences and Engineering Research Council of Canada (RGPIN-2023-03237).

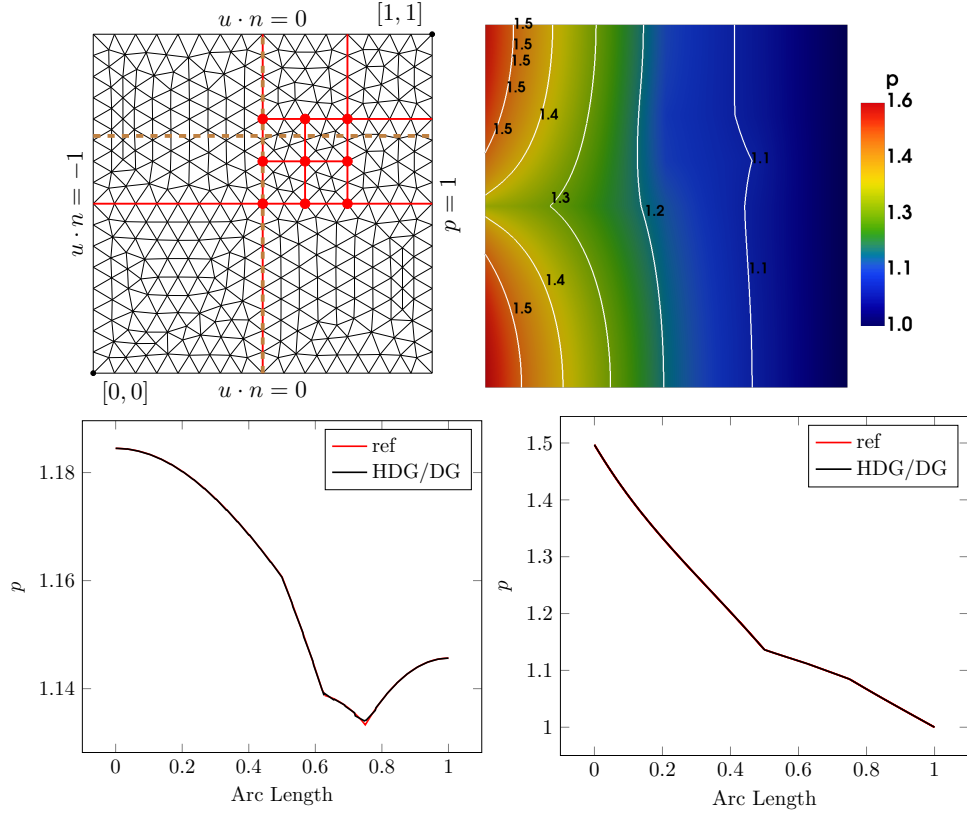


Figure 9: The regular fault network problem as described in section 6.4. (Top left) Problem setup together with the initial mesh. Conducting faults are depicted by red lines. To compare solutions of different discretizations we sample the pressure along the brown dashed lines, $x = 0.5$, which coincides with a fault, and $y = 0.75$. (Top right) The pressure distribution obtained by the HDG/DG method. (Bottom) Comparison of the HDG/DG pressure solution in terms of pressure values on a line $x = 0.5$ (left) and a line $y = 0.75$ (right) computed on a mesh with 2382 cells to the reference pressure solution computed using MFD on a mesh with approximately 1.1 million (triangular) cells [18].

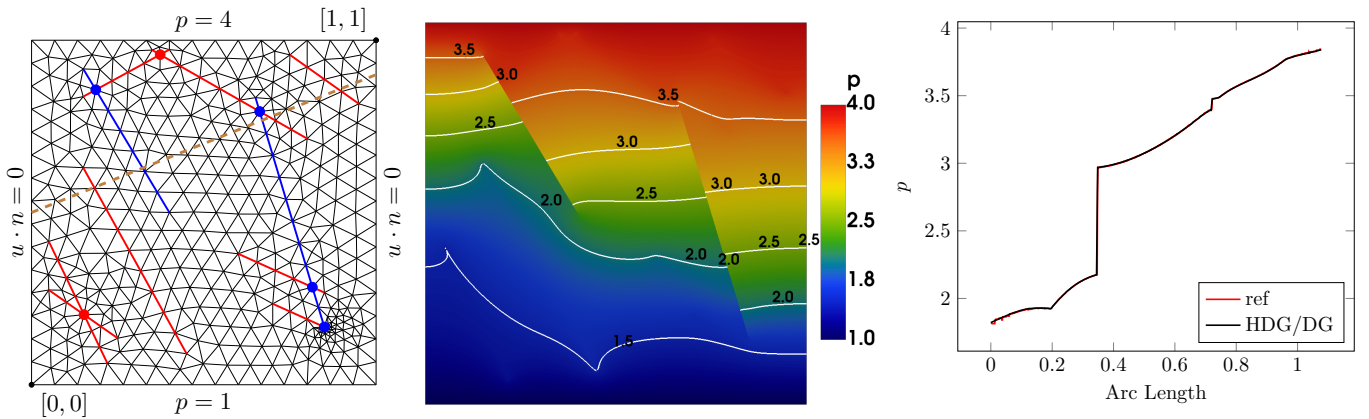


Figure 10: The complex fault network problem as described in section 6.4. (Left) Problem setup together with the initial mesh. Conducting/sealing faults are depicted by red/blue lines. To compare solutions of different discretizations we sample the pressure along the brown dashed line which crosses multiple conducting and sealing faults. (Center) The pressure distribution obtained by HDG/DG method. (Right) Comparison of the HDG/DG pressure solution computed on a mesh with 2744 cells to the reference pressure solution computed using MFD on a mesh with approximately 1.2 million (quadrilateral/triangular) cells [18].

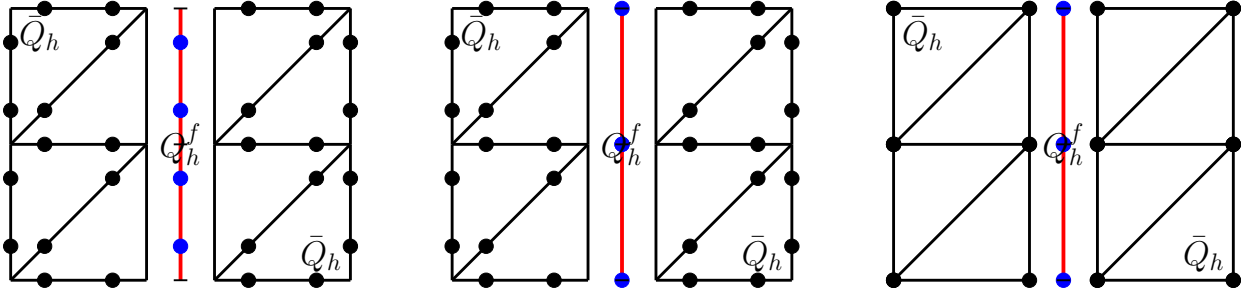


Figure 11: Schematic of the face function spaces involved in the HDG/DG (left), HDG/CG (center), and EDG/CG (right) discretizations of a single conducting fault problem. The black and blue nodes indicate the degrees of freedom of \bar{Q}_h and Q_h^f , respectively, when linear ($k = k_f = 1$) elements are used on the faces.

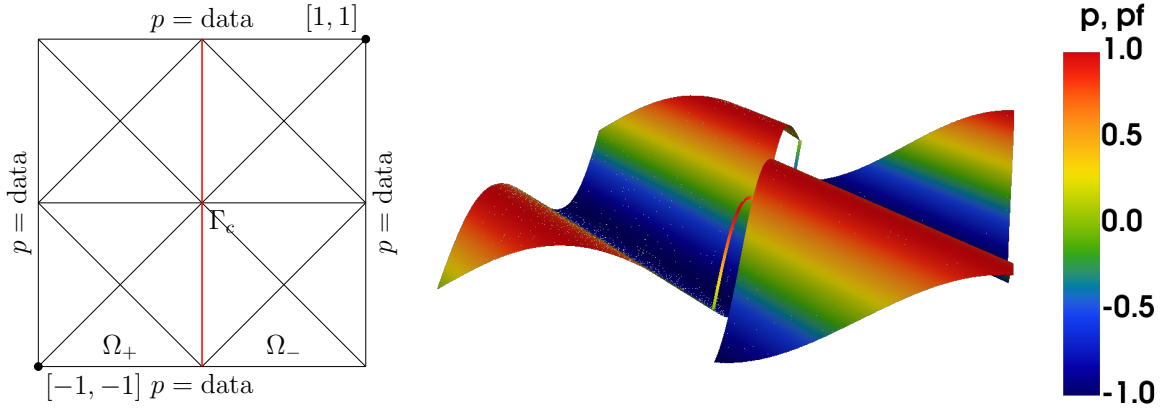


Figure 12: Setup of the error convergence study for comparing HDG/DG, HDG/CG and EDG/CG discretizations. (Left) Geometry with a conducting fault in red, and a sample mesh. (Right) Discrete pressures on the finest mesh ($h = 1/64$) with the HDG/DG discretization choosing $k = k_f = 1$.

A Two alternative hybridizable discretizations

In section 3 we presented the HDG/DG discretization for the porous media with faults problem eq. (1). We now present two alternative, but very similar, discretizations. These are: (i) the hybridizable discontinuous Galerkin/continuous Galerkin (HDG/CG) method; and (ii) the embedded discontinuous Galerkin/continuous Galerkin method (EDG/CG).

Both discretizations consider a continuous approximation to the pressure in the fault; the finite element space Q_h^f in eq. (4) is replaced by

$$Q_h^f := \{q_h^f \in C^0(\Gamma_c) : q_h^f \in P_{k_f}(F) \forall F \in \mathcal{F}_c^f\}, \quad k_f = k.$$

For the HDG/CG scheme, the remaining spaces in eq. (4) are the same. For the EDG/CG scheme, following [20], we replace \bar{Q}_h in eq. (4) by

$$\bar{Q}_h := \{\bar{q}_h \in C^0((\cup_{F \in \mathcal{F}} F) \setminus \Gamma_c) : \bar{q}_h \in P_k(F) \forall F \in \mathcal{F} \setminus \mathcal{F}_c^f\}.$$

An illustration of the face spaces of the different discretizations is shown in fig. 11 for the conducting fault case.

To demonstrate approximation properties of the three discretizations we consider for simplicity a problem setup with a single conducting fault. Specifically, we let $\Omega = (-1, 1)^2$ where the domain is split by a vertical fracture, cf. fig. 12. We define the exact solution p and p_f as follows

$$p|_{\Omega_+} = \sin(\pi(x + y)), \quad p|_{\Omega_-} = \cos(\pi(x + y)), \quad p_f = \sin(\pi(x - y)).$$

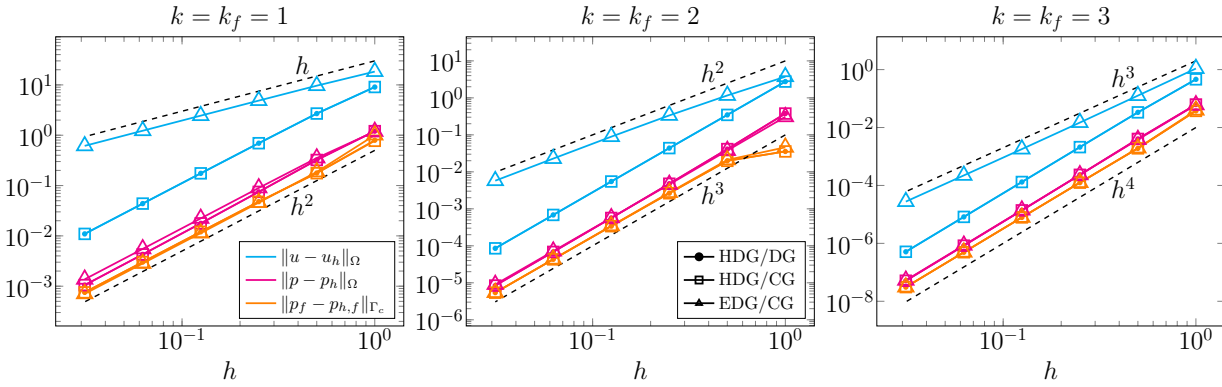


Figure 13: Rates of convergence of the HDG/CG, EDG/CG and HDG/CG approximations to the solution of the problem described in A. Results due to a particular scheme are encoded by a specific marker. Colors represent the errors in the different quantities.

We prescribe p and p_f as boundary data on $\partial\Omega$ and $\partial\Gamma_c = (\partial\Gamma_c)^D$, respectively. The model parameters are set as $\alpha_f = 2$, $\xi = 0.75$, $\kappa_f = 3$ and we take a discontinuous permeability κ such that $\kappa|_{\Omega_+} = 5$, $\kappa|_{\Omega_-} = 4$.

Figure 13 summarizes the errors and rates of convergence using HDG/DG, HDG/CG and EDG/CG methods with $k = 1, 2, 3$ and $k_f = k$. As expected from an EDG discretization, the error in u_h is $\mathcal{O}(h^k)$ (see, for example, [15]). The errors in other variables are $\mathcal{O}(h^{k+1})$. For HDG/CG, errors in all variables are $\mathcal{O}(h^{k+1})$, as expected.

References

- [1] C. Alboin, J. Jaffre, J. Roberts, and C. Serres. Domain decomposition for flow in porous media with fractures. In *14th Conference on Domain Decomposition Methods in Sciences and Engineering*, 1999.
- [2] D. N. Arnold. An interior penalty finite element method with discontinuous elements. *SIAM J. Numer. Anal.*, 19(4):742–760, 1982.
- [3] D. N. Arnold, F. Brezzi, B. Cockburn, and L. D. Marini. Unified analysis of discontinuous Galerkin methods for elliptic problems. *SIAM J. Numer. Anal.*, 39(5):1749–1779, 2002.
- [4] T. Bærlund, J. J. Lee, K.-A. Mardal, and R. Winther. Weakly imposed symmetry and robust preconditioners for Biot’s consolidation model. *Computational Methods in Applied Mathematics*, 17(3):377–396, 2017.
- [5] M. F. Benedetto, A. Borio, F. Kyburg, J. Mollica, and S. Scialò. An arbitrary order mixed virtual element formulation for coupled multi-dimensional flow problems. *Comput. Methods Appl. Mech. Engrg.*, 391:Paper No. 114204, 27, 2022.
- [6] S. C. Brenner. Poincaré-Friedrichs inequalities for piecewise H^1 functions. *SIAM J. Numer. Anal.*, 41(1):306–324, 2003.
- [7] S. C. Brenner and L. R. Scott. *The Mathematical Theory of Finite Element Methods*. Springer, 3rd edition, 2010.
- [8] F. Brezzi, K. Lipnikov, and V. Simoncini. A family of mimetic finite difference methods on polygonal and polyhedral meshes. *Mathematical Models and Methods in Applied Sciences*, 15(10):1533–1551, 2005.
- [9] E. Burman, P. Hansbo, and M. G. Larson. A cut finite element method for a model of pressure in fractured media. *Numer. Math.*, 146(4):783–818, 2020.

- [10] T. M. Cavalcante, F. R. L. Contreras, and D. K. E. Carvalho P. R. M. Lyra. A multipoint flux approximation with diamond stencil finite volume scheme for the two-dimensional simulation of fluid flows in naturally fractured reservoirs using a hybrid-grid method. *Internat. J. Numer. Methods Fluids*, 92(10):1322–1351, 2020.
- [11] F. Chave, D. A. Di Pietro, and L. Formaggia. A hybrid high-order method for passive transport in fractured porous media. *Int. J. Geomath.*, 10:12, 2019.
- [12] S. Chen, X. Li, and H. Rui. The finite volume method based on the Crouzeix-Raviart element for a fracture model. *Numer. Methods Partial Differential Equations*, 35(5):1904–1927, 2019.
- [13] B. Cockburn, B. Dong, and J. Guzmán. A superconvergent LDG-hybridizable Galerkin method for second-order elliptic problems. *Math. Comp.*, 77(264):1887–1916, 2008.
- [14] B. Cockburn, J. Gopalakrishnan, and R. Lazarov. Unified hybridization of discontinuous Galerkin, mixed, and continuous Galerkin methods for second order elliptic problems. *SIAM J. Numer. Anal.*, 47(2):1319–1365, 2009.
- [15] B. Cockburn, J. Guzmán, S.-C. Soon, and H. K. Stolarski. An analysis of the embedded discontinuous Galerkin method for second-order elliptic problems. *SIAM J. Numer. Anal.*, 47(4):2686–2707, 2009.
- [16] D. A. Di Pietro and A. Ern. *Mathematical aspects of discontinuous Galerkin methods*, volume 69 of *Mathématiques et Applications*. Springer-Verlag Berlin Heidelberg, 2012.
- [17] S. Du and F. J. Sayas. *An Invitation to the Theory of the Hybridizable Discontinuous Galerkin Method: Projections, Estimates, Tools*. Cham: Springer International Publishing AG, 2019.
- [18] B. Flemisch, I. Berre, W. Boon, A. Fumagalli, N. Schwenck, A. Scotti, I. Stefansson, and A. Tatomir. Benchmarks for single-phase flow in fractured porous media. *Advances in Water Resources*, 111:239–258, 2018.
- [19] V. Girault and P.-A. Raviart. *Finite element approximation of the Navier-Stokes equations*, volume 749 of *Lecture Notes in Mathematics*. Springer-Verlag, Berlin-New York, 1979.
- [20] S. Güzey, B. Cockburn, and H.K. Stolarski. The embedded discontinuous Galerkin method: application to linear shell problems. *International journal for numerical methods in engineering*, 70(7):757–790, 2007.
- [21] M. Kuchta. Assembly of multiscale linear PDE operators. In *Numerical Mathematics and Advanced Applications ENUMATH 2019: European Conference, Egmond aan Zee, The Netherlands, September 30-October 4*, pages 641–650. Springer, 2020.
- [22] J. J. Lee, T. Bui-Thanh, U. Villa, and O. Ghattas. Forward and inverse modeling of fault transmissibility in subsurface flows. *Computers & Mathematics with Applications*, 128:354–367, 2022.
- [23] H. Leng and H. Chen. Adaptive interior penalty hybridized discontinuous Galerkin methods for Darcy flow in fractured porous media. *IMA J. Numer. Anal.*, 44(4):2165–2197, 2024.
- [24] R. Li, Y. Zhang, J. Wu, and Z. Chen. Discontinuous finite volume element method for Darcy flows in fractured porous media. *J. Comput. Appl. Math.*, 381:Paper No. 113025, 18, 2021.
- [25] Y. Liu and Z. Xu. An interior penalty discontinuous Galerkin. method for an interface model of flow in fractured porous media. *arXiv preprint arXiv:2405.06874*, 2024.
- [26] A. Logg, K-A. Mardal, and G. Wells. *Automated solution of differential equations by the finite element method: The FEniCS book*, volume 84. Springer Science & Business Media, 2012.

- [27] V. Martin, J. Jaffre, and J.E. Roberts. Modeling fractures and barriers as interfaces for flow in porous media. *SIAM Journal on Scientific Computing*, 26(5):1667–1691, 2005.
- [28] G. Pichot, J. Erhel, and J. R. de Dreuzy. A mixed hybrid mortar method for solving flow in discrete fracture networks. *Appl. Anal.*, 89(10):1629–1643, 2010.
- [29] G. Pichot, J. Erhel, and J.-R. de Dreuzy. A generalized mixed hybrid mortar method for solving flow in stochastic discrete fracture networks. *SIAM J. Sci. Comput.*, 34(1):B86–B105, 2012.
- [30] B. Rivière. *Discontinuous Galerkin methods for solving elliptic and parabolic equations*, volume 35 of *Frontiers in Applied Mathematics*. Society for Industrial and Applied Mathematics (SIAM), Philadelphia, 2008.
- [31] L. Zhao and E. Chung. An adaptive discontinuous Galerkin method for the Darcy system in fractured porous media. *Comput. Geosci.*, 26(6):1581–1596, 2022.